# Speciation of toxic pollutants in Pb/Zn smelter slags by X-ray Absorption Spectroscopy in the context of the literature

Dan Ting Chen, Amitava Roy, Yu Qian Li, Anna Bogush, Wing Yin Au, Julia A. Stegemann

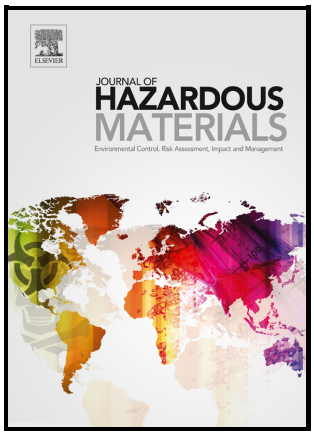


PII: S0304-3894(23)01656-4

DOI: https://doi.org/10.1016/j.jhazmat.2023.132373

Reference: HAZMAT132373

To appear in: *Journal of Hazardous Materials*

Received date: 26 June 2023
Revised date: 21 August 2023
Accepted date: 22 August 2023

Please cite this article as: Dan Ting Chen, Amitava Roy, Yu Qian Li, Anna Bogush, Wing Yin Au and Julia A. Stegemann, Speciation of toxic pollutants in Pb/Zn smelter slags by X-ray Absorption Spectroscopy in the context of the literature, *Journal of Hazardous Materials,* (2023) doi:https://doi.org/10.1016/j.jhazmat.2023.132373

# Speciation of toxic pollutants in Pb/Zn smelter slags by X-ray Absorption Spectroscopy in the context of the literature

Dan Ting Chen[a], Amitava Roy[b], Yu Qian Li[a], Anna Bogush[a], Wing Yin Au[a], and Julia A. Stegemann[a1]

[a] *Department of Civil, Environmental and Geomatic Engineering (CEGE), University of College London (UCL), Chadwick Building, Gower Street, London WC1E 6BT, UK*

[b] *Louisiana State University Center for Advanced Microstructures and Devices, Baton Rouge, LA 70806, USA*

## Abstract

Pb/Zn smelter slag is a hazardous industrial waste from the Imperial Smelting Process (ISP). The speciation of zinc, lead, copper and arsenic in the slag controls their recovery or fate in the environment but has been little investigated. X-ray Absorption Spectroscopy (XAS) was applied to this complex poorly crystalline material for the first time to gain new insights about speciation of elements at low concentration. Zn, Cu, As K-edge and Pb L3-edge XAS was carried out for a Pb/Zn slag from a closed ISP facility in England, supported by Fe, S and P K-edge XAS. Results are presented in the context of a full review of the literature. X-ray fluorescence showed that concentrations of Zn, Pb, Cu and As were 8.4, 1.6, 0.48 and 0.45 wt.%, respectively. Wüstite (FeO) was the only crystalline phase identified by X-ray diffraction, but XAS provided a more complete understanding of the matrix. Zn was found to be mainly present in glass, ZnS, and possibly solid solutions with Fe oxides; Pb was mainly present in glass and apatite minerals (e.g., $Pb_5(PO_4)_3OH$); Cu was mainly speciated as $Cu_2S$, with some metallic Cu and a weathering product, $Cu(OH)_2$; As speciation was likely dominated by arsenic (III) and (V) oxides and sulfides.

## 1. Introduction

Zinc and lead are the two most widely used non-ferrous metals after aluminium and copper, with global production of 13.9 and 12.4 Mt in 2021, respectively (ILZSG, 2022). Sustainability considerations have resulted in dominance of hydrometallurgical production for both metals, but about 10-20% of global Zn and Pb are still obtained by pyrometallurgical processing (Nowińska and Zdzisław, 2017). Of the pyrometallurgical methods, the Imperial Smelting Process (ISP, also called 'blast furnace process') has important industrial significance for simultaneous production of zinc and lead, mainly from mixed zinc and lead sulfide ores, and has a long history of use since 1959 (Morgan, 1968, Cusano et al., 2017). However, 600-900 kg of Pb/Zn smelter slag are generated as a main byproduct for every tonne of Zn produced (Cusano et al., 2017). The state of knowledge about metallurgical slags in general is thoroughly discussed by Piatak and Ettler (2021).

Based on the assumption that 10% of the 350 Mt of global zinc production between 1960 and 2017 (based on calculations by Sverdrup et al. (2019)) was by ISP smelters, it can be estimated that over 20 Mt of Pb/Zn smelter slag were produced in this period. Although most ISP smelters in North America and Europe have been closed, about 1 Mt/y of Pb/Zn smelter slag continues to be produced by those remaining elsewhere, i.e., in India (Prasad and Ramana, 2016), China (Garside, 2022, Luo et al., 2019), Japan (Azuma, 2007), and Poland (Nowinska, 2020, Kicińska, 2020, Cusano et al., 2017).

[1]Corresponding author.
E-mail address: j.stegemann@ucl.ac.uk (J.A. Stegemann).

Zn smelter slag can also be generated as a by-product of other pyrometallurgical processing (e.g., Waelz process and slag fuming processes) of mainly secondary materials, e.g., dust from electric arc steelmaking and ashes, bottom and top dross from galvanising industries (Cusano et al., 2017). Likewise, Pb smelter slag can be generated as a by-product of other pyrometallurgical processes, mainly direct smelting of primary lead concentrates and some secondary material (e.g., lead scrap and lead-acid batteries) (Cusano et al., 2017).

Pb/Zn slags have been widely utilised, e.g., in China and Poland (Nowińska and Zdzisław, 2017) and India (Agrawal et al., 2004). Their high concentrations of cement elements, mainly Fe, Ca, Si and Al, have suggested a potential for recycling in construction materials. Pb/Zn slags are used as concrete aggregates (Babu et al., 2022, Reddy et al., 2020, Kore, 2020, Patil et al., 2018, Tripathi and Chaudhary, 2016, Prasad and Ramana, 2016, De Angelis and Medici, 2012, Weeks et al., 2008, Barna et al., 2004, Helios-Rybicka, 1997), inorganic geopolymer binders (Nath, 2020, Leuchtenmueller et al., 2020, Xia et al., 2019, Onisei et al., 2012), and in bricks (Hu et al., 2014) and tile glazes (Bayer Ozturk et al., 2020).

Notwithstanding that utilization of Pb/Zn smelter slags is practiced elsewhere, they are defined as hazardous wastes by the European List of Wastes (10 04 01* and 10 05 01*) (Commission Decision, 2000/532/EC) due to their high concentrations of toxic metals, including Zn, Pb, Cu, As, etc.. The fate of these toxic metals in utilisation applications and also disposal scenarios is an environmental concern. There is also the potential to recover these metals as secondary raw materials. Only a few investigations of toxic metal extraction and recovery have been conducted, including hydrometallurgical recovery (Song et al., 2019). The fate and recoverability of metals in slags are closely linked to their speciation.

Previous investigations of the speciation of Zn, Pb, Cu and As (2.3) have usually been conducted using X-ray diffraction (XRD) or sometimes scanning electron microscopy (SEM) with energy dispersive X-ray spectroscopy (EDS) or electron probe microanalysis (EPMA). However, phases determined by XRD must be crystalline and present in high enough concentration (~ 2%) (Chen et al., 2021), and it is not possible to know whether they contain elements of interest in solid solution. X-ray absorption spectroscopy (XAS) is a powerful technique for direct molecular-level study of specific elements in complex materials, irrespective of their crystallinity and even at low concentrations (i.e., a few hundreds of mg/kg). The aim of the present study was to determine the speciation of Zn, Pb, Cu and As in Pb/Zn smelter slag based on 1) a thorough review of the literature on this subject, and 2) Zn, Cu and As K-edge, and Pb L3-edge XAS, with complementary Fe, S and P K-edge XAS, of a sample of ISP Pb/Zn smelter slag, also in comparison with actual and theoretical spectra of reference materials containing these elements.

# 2. Pb/Zn Smelter Slag

## 2.1. Formation of Pb/Zn smelter slag

Figure 1 presents a flow diagram for the typical ISP. The feed to this process mainly contains Pb and Zn sulfides from mining, and some secondary materials, such as sludge and dust from steelmaking (Bernasowski et al., 2017). The metal sulfide concentrates are oxidised into impure metal oxides (known as ‘zinc calcine’) during roasting, to remove most of sulfur and to agglomerate the fine flotation products. The zinc calcine is fed to the ISP furnace, which reduces metal oxides into metallic Pb and Zn vapour. The Zn vapour is then condensed and cooled before refining for commercial uses. The molten material, Pb/Zn slag and metallic Pb, remains in the bottom of the furnace. Lead bullion is separated from the slag, and the slag is then quenched and granulated by water. Other pyrometallurgical processes that produce Zn and Pb smelter slags follow similar reaction processes including oxidation, followed by reduction.

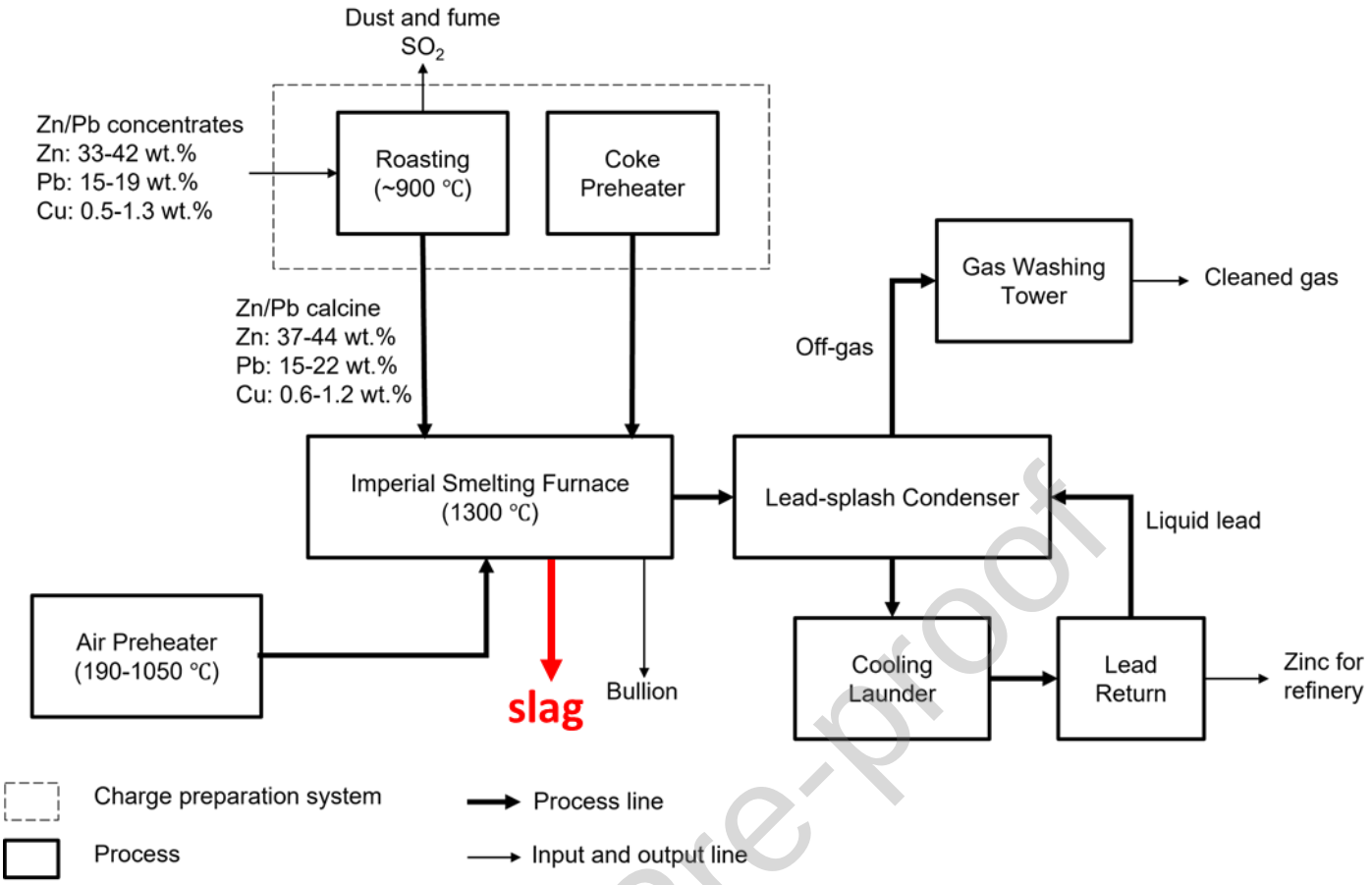


Figure 1. Schematic Diagram of the Imperial Smelting Process (ISP) for Zn production (Zhao, 2013, Taylor and Traulsen, 1988, Meek, 1979).

## 2.2. Elemental composition of smelter slags from lead and/or zinc production

Elemental compositions of a total of 56 smelter slags from production of Pb and/or Zn found in 39 papers were collected (Supplement File A). Figure 2 shows box charts for major matrix elements and elements of interest from the literature.

In Figure 2, Fe, Ca, Si, Zn and Al can be observed to be the dominant elements in the Pb/Zn slag matrix, with median concentrations of 20, 10, 10, 7 and 3.5% by mass, respectively. Median concentrations of 7% Zn, 0.7% Pb, 0.4% Cu, and 0.2% As (by mass) were collected for 55, 51, 29, and 29 samples, respectively. The inset bubble chart shows approximately log normal distributions for the concentrations of Zn, Pb and As, but not for Cu, which is difficult to rationalise considering the relatively lower sample numbers. One-way analysis of variance (ANOVA) showed no significant difference between the mean values, at the 5% level, among all three types of slags for all elements, except that Al has a lower mean in Pb slags, and Fe has a lower mean in Zn slags. The ANOVA results are summarised in Supplement File A.

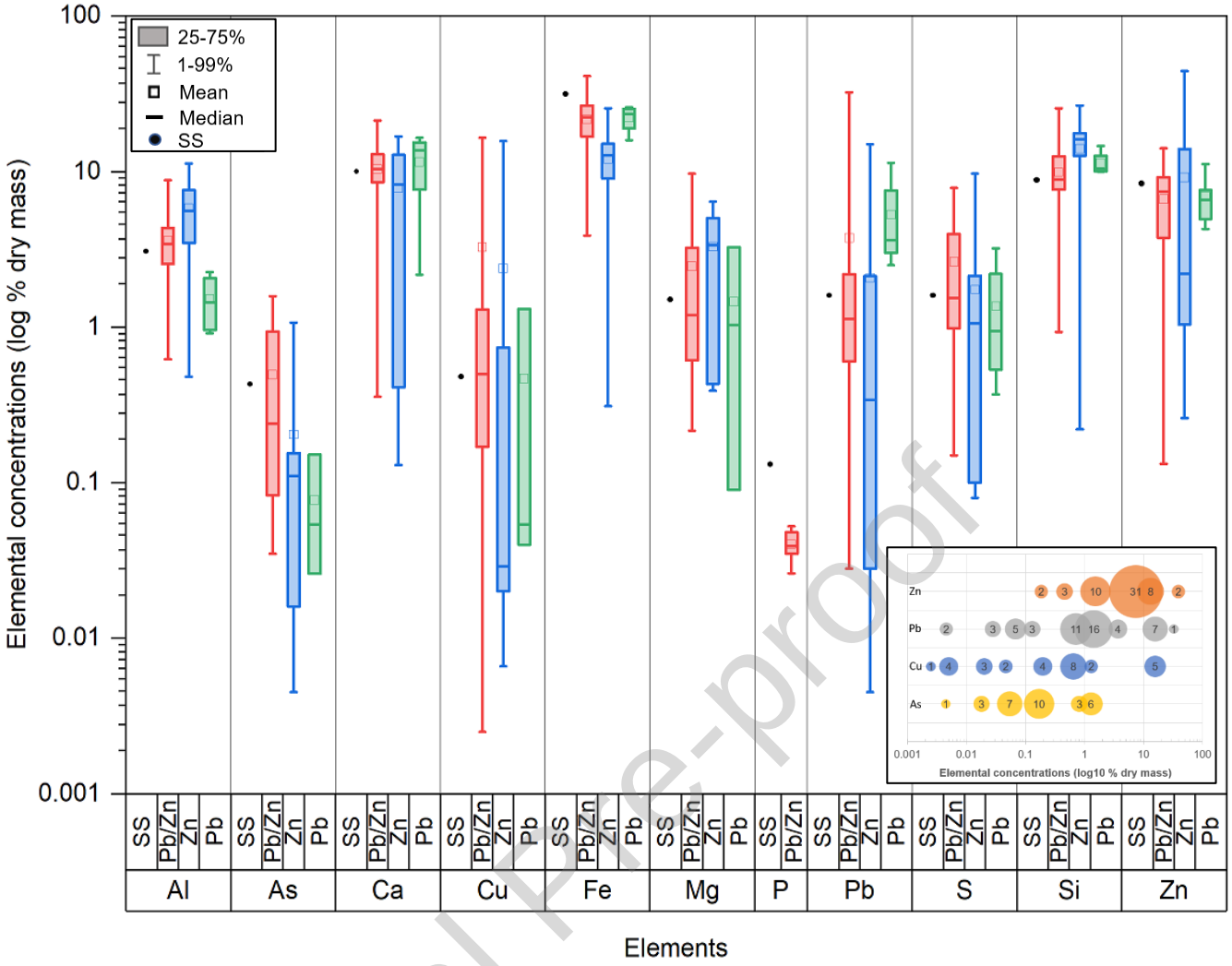


Figure 2. Box charts for concentrations of major and minor elements measured in smelter slags from Pb and/or Zn production in the literature and our sample (SS) by X-ray fluorescence (XRF). The inset bubble charts show the distribution of the concentrations of the elements of interest over their ranges, with the number of samples in represented by each bubble. Only major constituent elements (>1%) and those of interest for this study are presented here; raw data for all elements from the literature can be seen in Supplement File A, and raw data for 64 elements in our sample (SS) by three methods, i.e., XRF, conventional total acid digestion (TAD) and conventional aqua-regia digestion (ARD), can be seen in Supplement File B. The 39 literature sources are Atzeni et al. (1996), Morrison et al. (2003), Barna et al. (2004), Puziewicz et al. (2007), Weeks et al. (2008), Piatak and Seal II (2010), Yang et al. (2010), de Andrade Lima and Bernardez (2011), De Angelis and Medici (2012), Onisei et al. (2012), Alex et al. (2013), Adamczyk and Nowak (2013), Tripathi et al. (2013), Tyszka et al. (2014), Hu et al. (2014), Ettler and Johan (2014), Wang et al. (2015), Prasad and Ramana (2016), Tripathi and Chaudhary (2016), Morrison et al. (2016), Yin et al. (2016), Li et al. (2017), Patil et al. (2018), Xia et al. (2019), Song et al. (2019), Bayer Ozturk et al. (2020), Leuchtenmueller et al. (2020), Reddy et al. (2020), Kicińska (2020), Kore (2020), Luo et al. (2020), Nowinska (2020), Nath (2020), Ettler et al. (2020), Sajn et al. (2020).

## 2.3. Mineral composition of smelter slags from production of lead and/or zinc

The mineralogical compositions of 23 Pb/Zn slags, 12 Zn slags and 5 Pb slags were identified in a total of 23 previous studies using XRD, SEM/EDS, EPMA or Raman spectroscopy. These slags are usually glassy, since they were quenched, and have a dark grey colour because of a high iron content; nevertheless, various crystalline phases have

been observed, which are summarised in Table 1 (with more detailed information in Supplement File C). The results in the literature, show that the slags might contain a mixture of phases that derived from the original ore concentrate, or formed during roasting, metal reduction, or subsequent weathering.

For the major elements, the identified Fe and Ca-bearing phases were similar between Pb/Zn slags and Zn slags, including remaining ore minerals, and roasting, reduction and/or weathering products. Only roasting products were found in the Pb slags. Sulfides were the dominant S-bearing phases found in all three types of slags.

Zn phases in Pb/Zn slags included sulfides remaining from the ore, oxides (mainly spinels) from roasting, and hydroxide weathering products. Similar Zn phases were found in Zn slags, apart from the spinels, and in Pb slags, apart from weathering products. Pb phases in Pb/Zn slags included sulfides from the ore, roasting products, including oxides, silicates, sulfates, and arsenates, and metallic Pb from the reduction step. No Pb phases were found in Zn slags, and Pb sulfides, oxides, and metallic Pb were identified in Pb slags. Cu was found as sulfides and weathering products in both Pb/Zn slags and Zn slags, while no Cu phases were identified in Pb slags. No As phases were found in either Pb/Zn slags or Zn slags, but arsenic-bearing apatite was identified in Pb slags.

Table 1. Mineralogical compositions of elements of interest in smelter slags from Pb and/or Zn production.

| Element | Pb/Zn slag | Zn slag | Pb slag |
|---|---|---|---|
| Zn | 17/23 [a] | 3/12 [a] | 5/5 [a] |
| | **Remaining ores** | | |
| | Sulfides: sphalerite, ZnS; wurtzite, ZnS*; | Sulfides, i.e., sphalerite, ZnS; wurtzite, ZnS*; | Sulfides: wurtzite ZnS*; |
| | **Roasting products** | | |
| | Spinels: franklinite, $ZnFe_2O_4$; gahnite, $ZnAl_2O_4$; zinc chromite $ZnCr_2O_4$*; | | Spinels: franklinite, $ZnFe_2O_4$; |
| | Other oxides: zincite, ZnO*; | Oxides: zincite, ZnO*; | |
| | Silicates: willemite, $Zn_2SiO_4$; hardystonite, $Ca_2ZnSi_2O_7$; petedunnite/pyroxene, $CaZnSi_2O_6$; | Silicates: willemite, $Zn_2SiO_4$*; hardystonite, $Ca_2Zn(Si_2O_7)$*; | Silicates: willemite, $Zn_2SiO_4$*; hardystonite, $Ca_2ZnSi_2O_7$; melilite, $Ca_2(Fe,Zn)_2Si_2O_7$; |
| | **Weathering products** | | |
| | Sulfate hydrates: ktenasite, $ZnCu_4(SO_4)_2(OH)_6{\cdot}6H_2O$; namuwite, $Zn_4SO_4(OH)_6{\cdot}4H_2O$*; | Sulfate hydrates: brianyoungite, $Zn_3(CO_3,SO_4)(OH)_4$*; bechererite $Zn_7Cu(OH)_{13}[SiO(OH)_3SO_4]$ *; Fraipontite, $(Zn,Al)_3(Si,Al)_2O_5(OH)_4$*; | / |
| Pb | 12//23 [a] | 0/12 [a] | 3/5 [a] |
| | **Remaining ores** | | |
| | Sulfides: galena, PbS; | / | Sulfides: galena, PbS*; |
| | **Roasting products** | | |
| | Oxides: lead oxide, PbO*; wulfenite, $PbMoO_4$*; | / | Oxides: lead oxide, PbO*; |

| | | | |
|---|---|---|---|
| | Silicates, $Pb_4Al_2(SiO_3)_7$; | | |
| | Sulfates, $PbSO_4$; | | |
| | Arsenates: mimetite-johnbaumite, $Pb_5[(AsO_4)_3Cl]$-$Ca_5(AsO_4)_3(OH)$*; | | |
| | **Reducing products** | | |
| | Metallic: Pb | / | Metallic: Pb |
| Cu | 6//23 [a] | 2/12 [a] | 0/5 [a] |
| | **Remaining ores** | | |
| | Sulfides: geerite, $Cu_8S_5$; covellite, CuS*; villamaninite, $(Cu,Ni,Co,Fe)S_2$*; chalcocite, $Cu_2S$*; chalcopyrite, $CuFeS_2$*, cubanite, $CuFe_2S_3$*; | Sulfides: Cu-Fe sulfides*; | / |
| | **Weathering products** | / | / |
| | Sulfates: ktenasite ($ZnCu_4(SO_4)_2(OH)_6\cdot 6H_2O$)<br>Nitrates: gerhardtite ($Cu_2(NO_3)(OH)_3$)) | Sulfates: bechereite, $Zn_7Cu(OH)_{13}[SiO(OH)_3SO_4]$*; | / |
| As | 0//23 [a] | 0/12 [a] | 1/5 [a] |
| | **Roasting products** | | |
| | / | / | Arsenates: mimetite-johnbaumite ($Pb_5[(AsO_4)_3Cl]$-$Ca_5(AsO_4)_3(OH)$) |
| Fe | 22/23 [a] | 10/12 [a] | 5/5 [a] |
| | **Remaining ores** | / | / |
| | Sulfides: pyrrhotite, FeS/ $Fe_{0.8\text{-}1}S$; troilite, FeS*; villamaninite, $(Cu,Ni,Co,Fe)S_2$*; chalcopyrite, $CuFeS_2$*; cubanite $CuFe_2S_3$*; | Sulfides: pyrrhotite, FeS/ $Fe_{0.8\text{-}1}S$; Cu-Fe sulfides*; | |
| | **Roasting products** | / | / |
| | Spinels: magnetite, $Fe_3O_4$; franklinite, $ZnFe_2O_4$; magnesioferrite, $MgFe_2O_4$; (Mg, Fe) $Al_2O_4$; calcium ferro oxide, $CaFe_2O_4$*;<br>Other oxides: wüstite, FeO; limenite, $FeTiO_3$;<br>Olivines: $(Ca,Fe,Mg)_2SiO_4$;<br>Silicates: kirschsteinite, $CaFeSiO_4$; clinopyroxene, $Ca(Mg,Fe)Si_2O_6$; melilite, $Ca_2MgSi_2O_7$+ $Ca_2FeSi_2O_7$; fayalite, $Fe_2SiO_4$*; $Ca(Fe_{0.69}Mg_{0.31})(SiO_4)$*; $CaFe_2SiO_4$*; | Oxides: hematite, $Fe_2O_3$;<br>Silicates: clinopyroxene, $Ca(Mg,Fe)Si_2O_6$; fayalite, $Fe_2SiO_4$; | Spinels: magnetite, $Fe_3O_4$*;<br>franklinite, $ZnFe_2O_4$; (Mg, Fe) $Al_2O_4$;<br>Other oxides: wüstite, FeO;<br>Olivines: $(Ca,Fe,Mg)_2SiO_4$;<br>Silicates: kirschsteinite, $CaFeSiO_4$*; clinopyroxene, $Ca(Mg,Fe)Si_2O_6$; melilite, $Ca_2(Fe,Zn)Si_2O_7$; |
| | **Reducing products** | | |
| | Metalic: Fe | Metalic: Fe | / |
| | **Weathering products** | | |
| | Tochilinite, $Fe^{2+}{}_{5-6}(Mg,Fe^{2+})_5S_6(OH)_{10}$; natrojarosite, $NaFe_3(SO_4)_2(OH)_6$*;<br>Goethite, $\alpha$-FeOOH*; | Goethite, $\alpha$-FeOOH; | |
| Ca | 16/23 [a] | 10/12 [a] | 4/5 [a] |

| | | | |
|---|---|---|---|
| | **Remaining ores and fluxing agents** | | |
| | Calcite, $CaCO_3$*; clinomimetite, $Ca_5(PO_4, CO_3)_3(OH)$; | Calcite, $CaCO_3$*; | / |
| | **Roasting products** | | |
| | spinels: $CaFe_2O_4$*; | | |
| | Olivines: $(Ca,Fe,Mg)_2SiO_4$; | | Olivines: $(Ca,Fe,Mg)_2SiO_4$; |
| | Silicates: kirschsteinite, $CaFeSiO_4$; clinopyroxene, $Ca(Mg,Fe)Si_2O_6$; petedunnite/pyroxene, $CaZnSi_2O_6$*; melilite, $Ca_2MgSi_2O_7$+ $Ca_2FeSi_2O_7$; plagioclase ((Na, K)$AlSi_3O_8$+$CaAl_2Si_2O_8$*; hardystonite, $Ca_2ZnSi_2O_7$; Fayalite, $Ca(Fe_{0.69}Mg_{0.31})(SiO_4)$*; wollastonite, $Ca_2[Si_2O_6]$*; | Silicates: clinopyroxene, $Ca(Mg,Fe)Si_2O_6$; plagioclase ((Na, K)$AlSi_3O_8$+$CaAl_2Si_2O_8$; hardystonite, $Ca_2ZnSi_2O_7$*; | Silicates: kirschsteinite, $CaFeSiO_4$*; clinopyroxene, $Ca(Mg,Fe)Si_2O_6$; hardystonite, $Ca_2ZnSi_2O_7$*; melilite, $Ca_2(Fe,Zn)Si_2O_7$; |
| | **Weathering products** | | |
| | gypsum, $CaSO_4{\cdot}2H_2O$*; riversideite, $Ca_5Si_6O_{16}(OH)$)*; | gypsum, $CaSO_4{\cdot}2H_2O$; | / |
| S | 12/23 [a] | 10/12 [a] | 2/5 [a] |
| | **Remaining ores** | | |
| | Sulfides: pyrrhotite, FeS/ $Fe_{0.8\text{-}1}S$; troilite, FeS*; wurtzite ZnS; sphalerite ZnS; marmatite, $Zn_{1-x}Fe_xS$*; galena PbS; geerite, $Cu_8S_5$; covellite, CuS*; chalcocite, $Cu_2S$*; chalcopyrite $CuFeS_2$*; cubanite, $CuFe_2S_3$*; | Sulfides: pyrrhotite, FeS/ $Fe_{0.8\text{-}1}S$; wurtzite ZnS*; sphalerite ZnS*; Cu-Fe sulfides*; | Sulfides: wurtzite ZnS*; galena, PbS; |
| | Roasting products | | |
| | Sulfates: $PbSO_4$; | / | / |
| | Weathering products | | |
| | Sulfates: tochilinite, $Fe^{2+}_{5-6}(Mg,Fe^{2+})_5S_6(OH)_{10}$; natrojarosite, $NaFe_3(SO_4)_2(OH)_6$*; gypsum, $CaSO_4{\cdot}2H_2O$; namuwite, $Zn_4SO_4(OH)_6{\cdot}4H_2O$*; ktenasite ($ZnCu_4(SO_4)_2(OH)_6{\cdot}6H_2O$); villamaninite, $(Cu,Ni,Co,Fe)S_2$*; | Sulfates: gypsum, $CaSO_4{\cdot}2H_2O$; brianyoungite, $Zn_3(CO_3,SO_4)(OH)_4$*; | / |

'a' refers to the number of samples for which specific metal phases were identified, out of the total collected samples, e.g., for Zn, 17/23 means that Zn phases were identified in 17 out of a total of 23 Pb/Zn slag samples.

* indicates phases only identified once.

/ indicates no findings.

Common phases have been highlighted in purple.

All mineral phases are listed in Supplement File C, including their techniques and sources, from the following references: Atzeni et al. (1996), Helios-Rybicka (1997), Ettler et al. (2001), Puziewicz et al. (2007), Weeks et al. (2008), Tyszka et al. (2014), Morrison et al. (2016), Sobanska et al. (2016), Yin et al. (2016), Li et al. (2017), Xia et al. (2019), Bayer Ozturk et al. (2020), Reddy et al. (2020), Kicińska (2020), Nowinska (2020), Ettler et al. (2020), Piatak and Seal II (2010), Yang et al. (2010), Song et al. (2019), de Andrade Lima and Bernardez (2011), Onisei et al. (2012), Ettler and Johan (2014), Zheng et al. (2015)

# 3. X-ray Absorption Spectroscopy

## 3.1. Materials Selection and Characterisation

The ISP Pb/Zn smelter slag used for our XAS study was provided by an anonymous UK source in 2015. This facility smelted sulfide ores containing sphalerite-galena-pyrite-rich bands interlayered with quartz-carbonate turbidites and

mudstones, from the McArthur River zinc-lead mine, Australia (Gigon et al., 2020). The granulated slag contains glassy black particles, which remain shiny after two to four decades of weathering at their disposal site.

Examination of our Pb/Zn smelter slag was supported by XAS of twelve Zn reference materials (listed in Figure 7), eight Pb reference materials (Figure 10), ten Cu reference materials (Figure 11), eight As reference materials (Figure 14), three Fe reference materials (Figure 4a), ten S reference materials (Figure 5a) and two P reference materials (Figure 6), selected based on review of the literature about ISP Pb/Zn smelter slags. They included five glassy materials: Darwin glass containing 1.7 % Fe by mass (Giuli et al., 2002), a Ground Granulated Blast Furnace Slag (GGBFS) containing 1.4 % S by mass (Roy, 2009), "IR-Xglass" containing 0.63 % Zn by mass (Carpenter et al., 2002), "Corning glass B" containing 0.57 % Pb and 2.13 % Cu by mass and "Corning glass C" containing 34.1.% Pb by mass (Vicenzi et al., 2002). XAS spectra for three Zn and two Cu reference materials reported in publications by others were also used in this work (as described in 3.2).

X-ray fluorescence (XRF), XRD, SEM-EDS and simultaneous thermal analysis (STA) were used to study the smelter slag elemental composition, crystalline phases, morphologies, and mass changes and energy flows as a function of temperature, respectively. The detailed sample preparation and analytical methods are described in Supplement File D.

## 3.2. Collection and analyses of X-ray absorption spectra

Zn K-edge, Pb $L_3$-edge, Cu K-edge and As K-edge XAS spectra for our Pb/Zn smelter slag and the reference materials for these elements (nine for Zn, eight for Pb, eight for Cu and eight for As) were collected on Beamline 18, at the Diamond Light Source, Oxfordshire, UK (Dent et al., 2009), except for AsS (also known as $A_4S_4$, realgar) and $NaAsO_2$, which were run at Louisiana State University's (LSU) synchrotron research facility, the J. Bennett Johnston, Sr., Centre for Advanced Microstructures and Devices (CAMD), USA. Fe, S and P K-edge XAS spectra (three for Fe, ten for S and two for P) for the smelter slag sample and the relevant reference materials were also collected at CAMD, USA.

Details for Diamond Beamline 18 are reported by Bogush et al. (2019), and those for CAMD are reported by Leng et al. (2019) and Roy and Stegemann (2017). The monochromator position was calibrated by assigning the first peaks of the first derivatives of the K-edge of Zn foil, L3-edge of Pb foil, K-edge of Cu foil, K-edge of As powder, Fe foil, S foil and P foil to 9.659, 13.036, 8.979, 11.860, 7.112 keV, 2.472 and 2.146, respectively. Except for the IR-Xglass and Corning glass B, the reference materials and Zn and Fe in the smelter slag were measured in transmission mode. The elements with lower concentrations in the smelter slag (i.e., Pb, Cu, As, S and P), and the two above-mentioned glasses, were recorded in fluorescence mode. Eight scans were merged to improve the signal-to-noise ratio.

Based on initial analysis, more XAS spectra were required and digitally collected from the cited papers (three for Zn and two for Cu). The Zn XANES K-edge spectrum for Nano $ZnFe_2O_4$ was collected in transmission mode using Si (111) monochromator at the Elettra Synchrotrone Trieste, Italy (Akhtar and Nadeem, 2008). The Zn K-edge XANES spectrum for $Ca_2ZnSi_2O_7$ was collected in transmission mode on beamline Balder, Sweden (Rissler et al., 2020). Zn K-edge XANES of a glass containing 2.6% Zn ("Glass2.6") was collected by Alloteau et al. (2021) in fluorescence mode on the SAMBA beamline of SOLEIL, France. The Cu K-edge XANES spectrum for $Cu_2O$ was recorded at the XAFS beamline of the Stanford Synchrotron Radiation Laboratory (SSRL), USA (Gaur et al., 2009), and Cu K-edge XAS spectra for $Cu_2S$ were measured in transmission mode on beamline SSRL 4-3, SSRL, USA (Newville, 2020).

Data analysis to make the raw data from Diamond, CAMD and the cited papers comparable was performed with the Demeter packages, including Athena and Artemis, following standard procedures (Ravel and Newville, 2005). The edge energies $E_0$ for the elements of interest in the smelter slag were compared with those for the reference materials, to establish oxidation state and select reference materials for fingerprinting (see Figures 8, 12 and 15), apart from Pb, which has a complex coordination and single oxidation state (+2). In the current study, $E_0$ was defined as the first peak

of the first derivative. Qualitative fingerprinting compared features in the XAS spectra of the elements of interest in the Pb/Zn smelter slag with those of the selected reference materials, including the “white line”, and subsequent variations in absorption as a function of energy. When fingerprinting identified more than one phase, quantitative analysis was conducted by least-squares linear combination fitting (LCF) of the spectra of the elements of interest in the Pb/Zn slag with selected reference material spectra, over the range from -20 eV below to 30 eV above the edge $E_0$ for XANES spectra, and from 3 to 11-12 $Å^{-1}$ of the wavenumber “k” for the EXAFS spectra. The results were presented with uncertainty (‘±’) and closeness ‘R-factor’ (Calvin, 2013). Reference materials that contributed to less than 3% of the fit were rejected. The LCF of the first derivative of Pb and Cu XANES was undertaken due to the poor features of their XANES spectra. Fingerprinting of Pb and As EXAFS spectra was not possible due to significant noise inherent to EXAFS of these elements.

# 4. Results

## 4.1. Elemental and mineralogical characterisation of the Pb/Zn smelter slag

The dots (labelled SS) in Figure 2 show the element concentrations measured in our Pb/Zn smelter slag sample by XRF. The major elements, ranked from largest to lowest concentration, were Fe (31 %), Ca (10 %), Si (8.8 %), Zn (8.4 %), Al (3.1%), S (1.6 %), Pb (1.6 %) and Mg (1.5 %), followed by minor elements Cu (0.48 %), As (0.45 %) and P (0.13 %), on a dry mass basis. Comparison with the median element concentrations in the literature in Figure 2 indicates that Ca, Si, Zn, Al, S, Mg, and Cu concentrations in our smelter slag were very similar. The Fe, As, and Pb concentrations of our smelter slag were within a factor of two of the median literature concentrations, and the P concentration was within an order of magnitude. Our smelter slag thus seems to have the elemental composition of a typical Pb/Zn slag. Full chemical analysis results for 64 elements is provided in Supplement File B.

The mineralogical composition of our smelter slag sample determined by XRD is shown in Figure 3 (left), with an inset showing the FTIR spectrum. The XRD pattern of the smelter slag shows one major crystalline phase: wüstite ($Fe_{0.925}O$, Crystallographic Open Database 96-900-9772). The peaks are broad and of low intensities, with an average crystallite size for wüstite of 250 Å. A broad hump is observed in the pattern centred at 31.4° 2θ due to the glassy matrix (Ettler et al., 2020). A few unidentified peaks remain. No Ca or Si-bearing compounds were identified by XRD, indicating that those elements are more likely present in the amorphous matrix of this slag. The broad peak seen in the FTIR pattern at 900 $cm^{-1}$ corroborates the glassy nature of our smelter slag and its low degree of polymerisation (Parke, 1974). Thermal analysis of the smelter slag showed no detectable mass loss due to carbonation, absorbed moisture or structural water, suggesting very little weathering.

The SEM/EDS results indicated that our smelter slag sample mainly contains glassy particles consisting of Ca, Fe, Zn, Si, Al, and O with impurities of other elements (e.g., Mg and S) (Spectra 1-4 and 7-10), and inclusions of Pb oxide, carbon, Pb (Spectra 6), Cu oxide with impurities of sulfides with impurities of As, Cu and Sb (Spectra 11-12) (Figure 3, middle and bottom). Tiny crystals (about 1µm) of mainly Fe and Zn were also observed in the glassy particles (Spectrum 5).

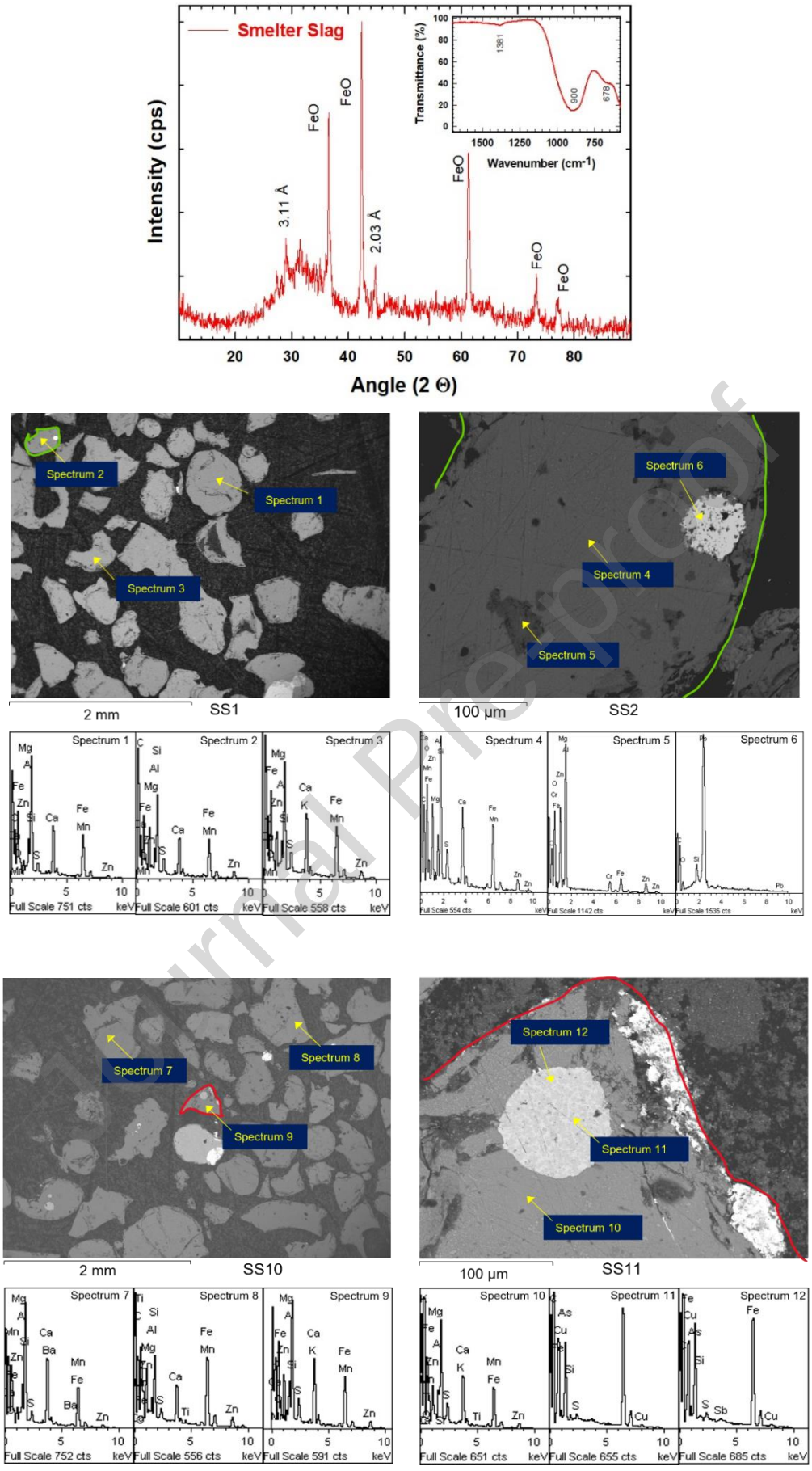


Figure 3. The powder X-ray diffraction (XRD) pattern of the Pb/Zn smelter slag sample with inset Fourier-transform infrared spectroscopy (FTIR) spectrum (top), and representative examples of Scanning Electron Microscopy with Energy Dispersive Spectroscopy (SEM-EDS) of the Pb/Zn smelter slag sample (middle and bottom). The same area is emphasized by curve with same colour (green and red), and the spots are pointed by arrows. The size of images and spot numbers are summarised in Table SC1.

## 4.2. Iron, sulfur and phosphorus K-edge X-ray Absorption Spectroscopy

Fingerprinting of the Fe K-edge XANES spectrum of our Pb/Zn smelter slag sample with those of wüstite (FeO), magnetite and Darwin Glass shows a close resemblance to that of FeO (Figure 4). (Sobanska et al., 2000) reported that some amount of substitution of Fe in FeO by Zn is possible. An Fe K-edge XANES spectrum of $Zn_xFe_{1-x}O$ could not be obtained, however its simulation with FEFF10 (Figure 4b, based on (Kas et al., 2021) shows that Zn substitution should result in a shift of the absorption edge to lower energy, with flattening of the inflections, even with ca. 10% Zn replacement. Any substitution in FeO by Zn in our smelter slag thus appears to be limited, as very little shift (<0.1 eV) in the Fe edge energy between standard FeO and our sample was seen. On the other hand, a large degree of solid solution between magnetite ($Fe_3O_4$) and franklinite ($ZnFe_2O_4$) can take place at high temperatures, and this may have occurred in the slag (Manceau et al., 2000, Sobanska et al., 2000). Linear combination fitting of the Fe K edge XANES spectrum for our smelter slag with our reference materials resulted in a best fit for 66±1% FeO, 21±2% Darwin Glass and 13±1% $Fe_3O_4$ with an R-factor of 6.9 x $10^{-4}$. All Fe-bearing sulfide phases were rejected by this fitting. The fitted combination is consistent with the XRD results. The inset in Figure 4a shows the Fourier transforms of the EXAFS spectra of the fitted phases. The distances of the first two shells for the smelter slag correspond well to those of FeO and $Fe_3O_4$, corroborating their presence.

Figure 5a shows the S K edge XANES spectra of our smelter slag sample and the S reference materials, including metal sulfides, a sulfate and GGBFS. The S K edge absorption energy shifts from ca. 2470 eV to ca. 2481 eV as the oxidation state increases from -2 (sulfide) to +6 (sulfate) (Myneni, 2002). This is evident in the peak positions, for example, of ZnS (a, 2472.52 eV) and $Fe_2(SO_4)_3.xH_2O$ (b, 2481.66 eV). The Pb/Zn smelter slag has a broad peak centred around 2474.45 eV and a sharper peak at 2481.38 eV. Its spectrum is remarkably similar to that of GGBFS (Roy, 2009), which is produced under very similar conditions and has similar peaks at 2475.29 eV and 2481.38 eV.

Figure 5b shows the result of linear combination fitting of our smelter slag with those of ten sulfur reference materials. The best fit is obtained with 44±2% GGBFS, 31±2% ZnS, 17±1% pyrrhotite ($Fe_{(1-x)}S$) and 8±3% $Fe_2(SO_4)_3.xH_2O$ with an R-factor of 0.02. It has been established that GGBFS has polysulfide species “frozen” in the glassy matrix due to quenching (Paris et al., 2001; Fleet et al., 2005), and it seems that a large part of the sulfur in the smelter slag is also present in the glassy matrix. Another major component is ZnS. These phases could not be detected by XRD, as glass is amorphous and ZnS was below the XRD detection limit of approximately 1%.

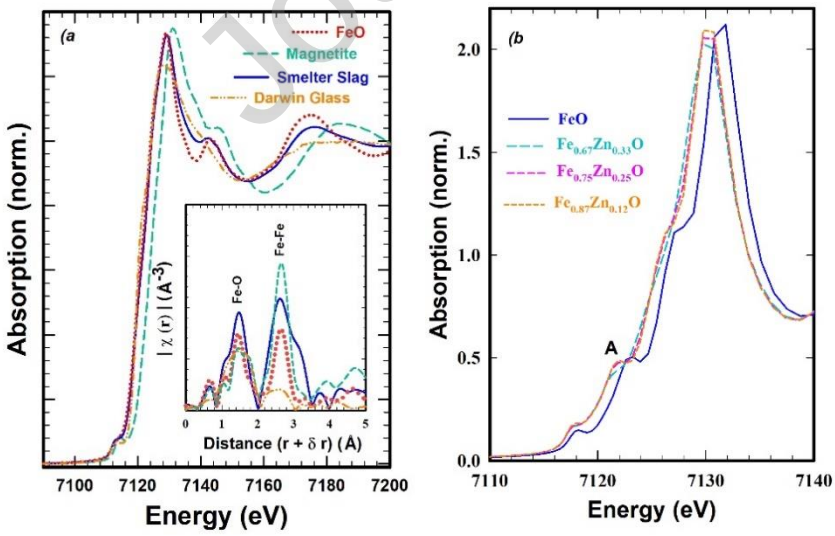


Figure 4. Normalised Fe K-edge XANES spectra for Pb/Zn smelter slag sample and three reference materials, with an inset of the Fourier Transforms of the EXAFS spectra (a), and calculated effect of Zn substitution in FeO on the XANES spectrum (Kas et al., 2021) (b).

Fingerprinting of the P K-edge XANES of our smelter slag with fluorapatite ($Ca_5(PO_4)_3F$) and hydroxyapatite ($Ca_5(PO_4)_3(OH)$) shows that phosphorus is present as apatite in the Pb/Zn smelter slag (Figure 6). The difference at B is attributable to a lower content of Ca in the slag since Ca in apatite is easily replaced by other elements (Franke and Hormes, 1995).

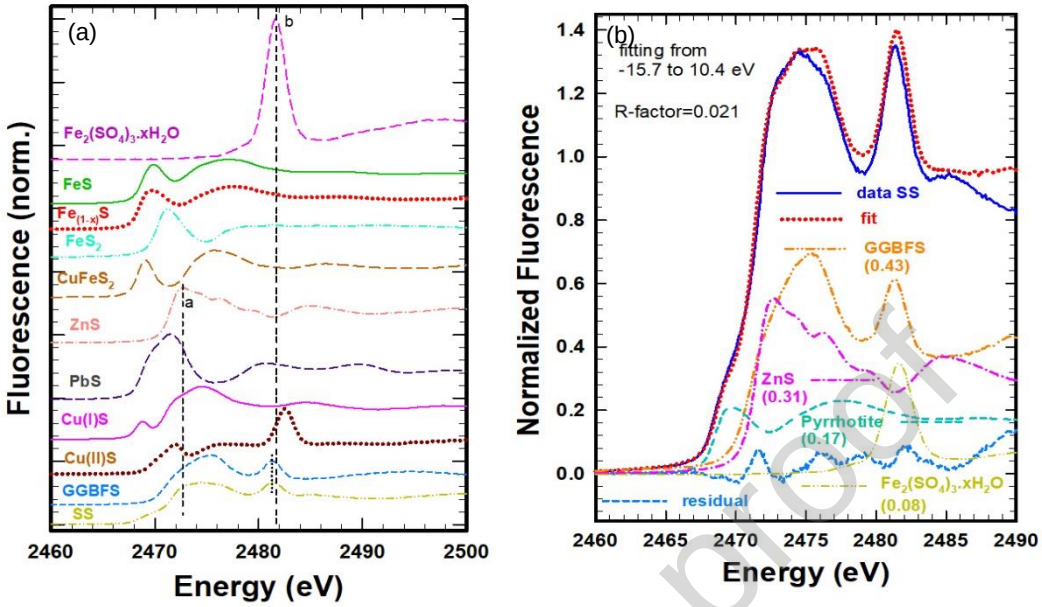


Figure 5. Normalised S K-edge XANES spectra for our Pb/Zn smelter slag sample and ten reference materials (a), and the best fit obtained by linear combination fitting (LCF) (b).

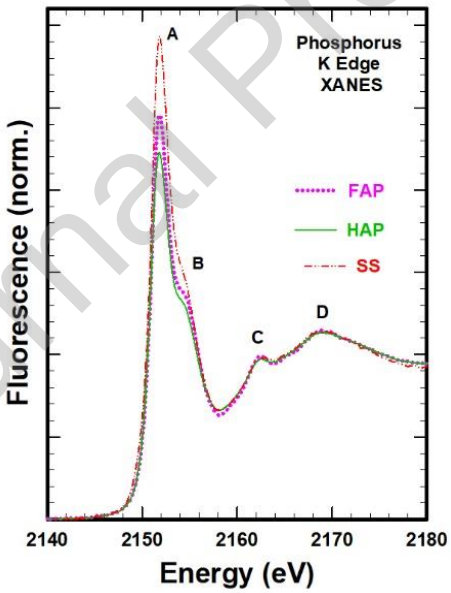


Figure 6. Normalised P K-edge XANES spectra for our Pb/Zn smelter slag sample, fluorapatite (FAP) and hydroxyapatite (HAP).

## 4.3. Zn K-edge X-ray absorption spectroscopy

### 4.3.1. Edge energy $E_0$

Figure 7 presents the Zn K-edge absorption edge energy ($E_0$) measured for the smelter slag sample among those of all twelve Zn reference materials with an oxidation state of +2, which were chosen based on previous studies. Although unidentified in previous studies, zinc arsenates ($Zn_2AsO_4OH{\cdot}7H_2O$ and $Zn_2AsO_4OH$) were included, as they are

conceivable products from the reaction of $As_2O_5$ and ZnO; $Zn_4Si_2O_7O_2H_2{\cdot}H_2O$ may be a product from hydration of $Zn_2SiO_4$ ((Vanaecker et al.) . Zn is tetrahedrally coordinated with oxygen atoms (in $ZnO_4$ units) in most of the Zn reference materials, but it is in five-fold and six-fold combined coordination (i.e., $Zn_2AsO_4(OH){\cdot}H_2O$ and $Zn_2AsO_4(OH)$, in combined $ZnO_5$ and $ZnO_6$ units) in two reference materials, and octahedral (i.e.,$ZnSO_4{\cdot}7H_2O$ in $ZnO_6$ units) in one; in ZnS it is tetrahedrally bonded with sulfur atoms (i.e., in $ZnS_4$ units). Reference materials with Zn in octahedral coordination tend to have a higher $E_0$ than those with tetrahedral coordination. Zn in IR-Xglass appears to be in tetrahedral coordination since its $E_0$ lies in the range of those of other tetrahedral compounds; this is in agreement with the results of McKeown et al. (2000). Likewise, Zn in Pb/Zn smelter slag has a relatively low $E_0$, suggesting tetrahedral coordination with an oxidation number of +2.

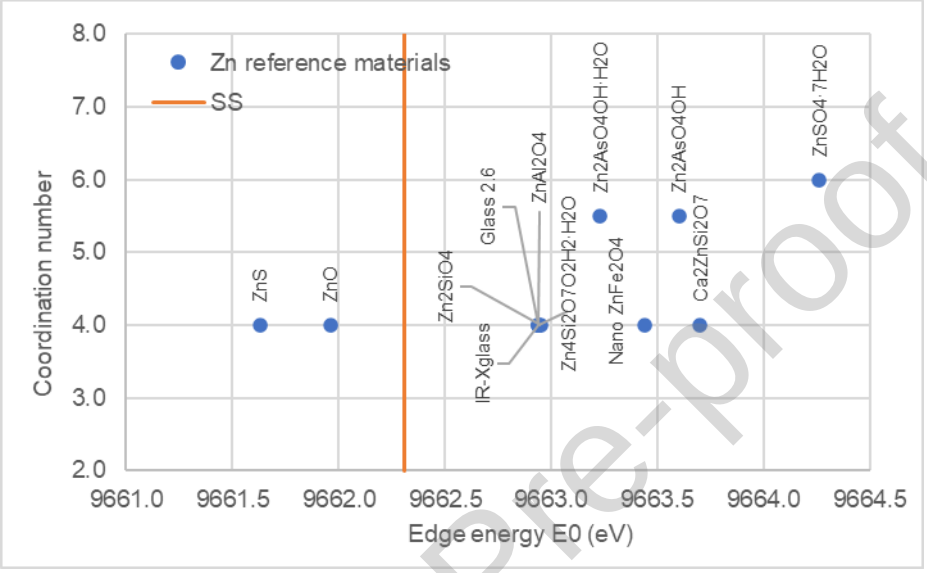


Figure 7. Edge energy of Zn K-edge XAS for the Pb/Zn smelter slag (SS) against coordination number, compared with all twelve Zn reference materials.

### 4.3.2. Fingerprinting and fitting of Pb/Zn smelter slag spectra with Zn reference material spectra

Figure 8a shows the Zn K-edge XANES spectrum of the Pb/Zn smelter slag sample, compared with those of the twelve Zn reference materials with various coordination geometries. The smelter slag XANES spectrum has a shoulder at ~9665.0 eV (‘a’) and a broad peak centered around ~9668.6 (‘b’). Similar peaks appear in the silicates (i.e., IR glass and Glass 2.6, $Zn_4Si_2O_7O_2H_2{\cdot}H_2O$ and $Zn_2SiO_4$), and/or nano $ZnFe_2O_4$ (see lines A and B), although their intensities differ.

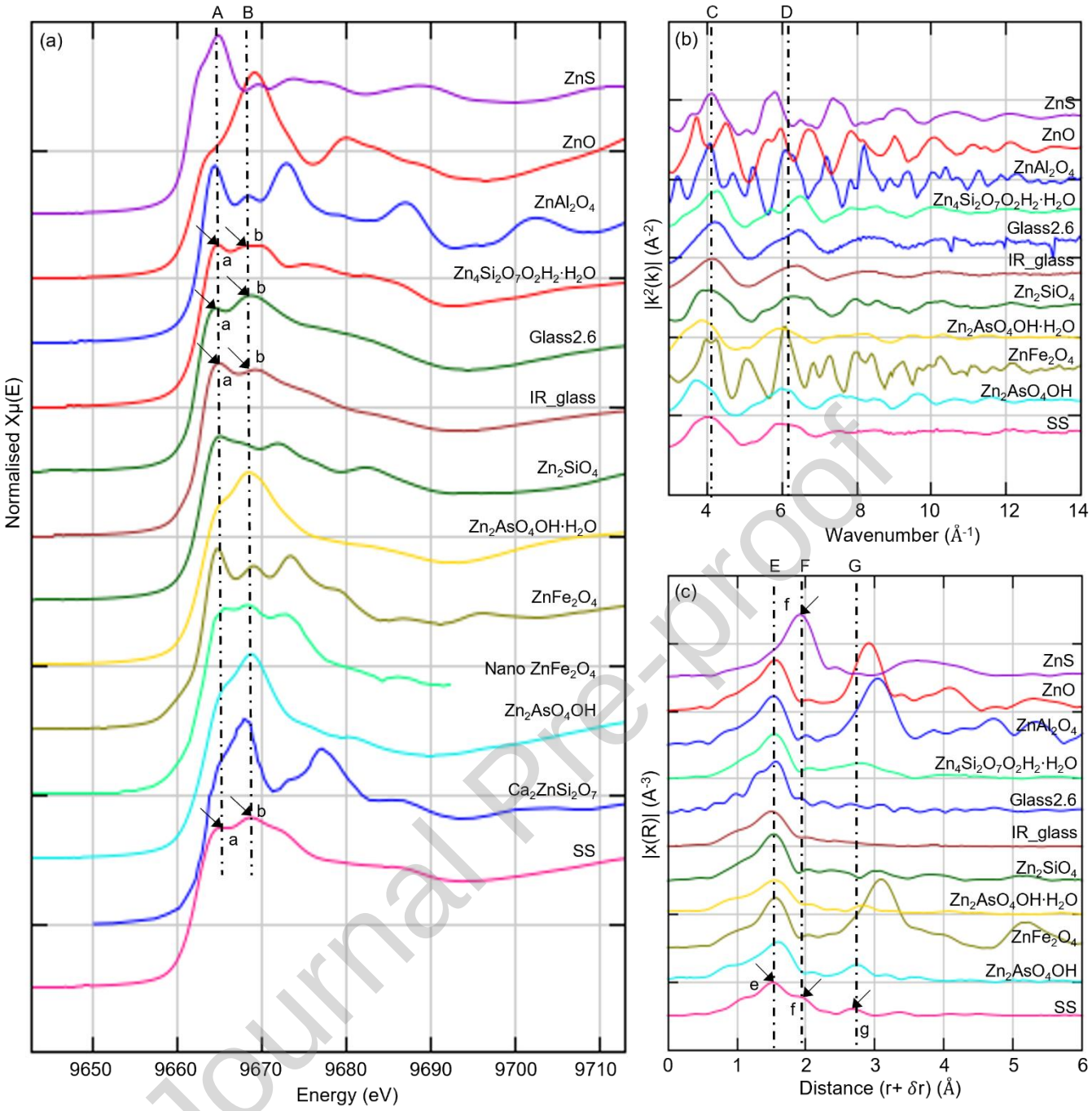


Figure 8. Normalised Zn K-edge XANES spectra for the Pb/Zn smelter slag sample (SS) and twelve Zn reference materials (a); Experimental Zn K-edge EXAFS spectra (b) and magnitude of Fourier Transforms (c) of Pb/Zn smelter slag and ten Zn reference materials (Fourier Transform spectra are uncorrected for phase shift).

Figures 8b and 8c present the Zn K-edge EXAFS spectrum for the Pb/Zn smelter slag sample, and its magnitude of Fourier transform with a k-weight of 2, compared with those for ten Zn reference materials; no EXAFS data for nano $ZnFe_2O_4$ and $Ca_2ZnSi_2O_7$ were available for comparison. The EXAFS spectrum for the smelter slag has a single sinusoidal oscillation (Figure 8b), which corresponds well to those in the spectra of the silicates (i.e., IR glass, Glass2.6, $Zn_4Si_2O_7O_2H_2{\cdot}H_2O$ and $Zn_2SiO_4$). The multiple sinusoidal oscillations in EXAFS spectra of ZnO, $ZnAl_2O_4$, $ZnFe_2O_4$ are not present in that of the slag. The Fourier Transform spectrum of the slag has a dominant peak at 1.52 Å ('e') and a shoulder at 1.92 Å ('f') in the first coordination sphere of the Fourier transform (Figure 8c), followed by a minor peak at 2.67 Å ('g'). The Fourier transform spectra of all Zn reference materials show similar nearest-neighboring coordination at roughly 1.52 Å ('e'), except for those of $Zn_2AsO_4(OH){\cdot}H_2O$ and ZnS, which have a major peak at a longer distance of

1.55 and 1.92 Å ('f'), respectively (Figure 8c). This suggests that ZnS contributes the small shoulder in the Fourier transform spectrum of the smelter slag. The Fourier transform spectra of ZnO, $ZnAl_2O_4$, $ZnFe_2O_4$ have a much stronger second peak at longer distances, which is also absent in that of the slag. Zn in the smelter slag is therefore more likely to be bonded with oxygen atoms and some sulfide atoms, both in tetrahedral coordination. The peak 'g' (Figure 8c) for the slag spectrum does not correspond to any peak of the shown reference materials with tetrahedral coordination, suggesting some other forms of Zn may be present, e.g., solid solutions with wüstite or iron spinels (as also suggested by the Fe-Zn crystals observed by SEM/EDS).

Figure 9 presents the best fit of the Zn K-edge XAS spectra for the Pb/Zn smelter slag with the spectra of the reference materials suggested by the fingerprinting. This demonstrates a good fit (R-factor = 0.002) of the XANES spectrum by 54±2% IR_Xglass, 29±3% ZnO and 17±3% ZnS in Figure 9a. This also indicates a relatively good fit (R-factor = 0.07) of the EXAFS spectrum by 81±1% IR_Xglass, 19±2% ZnS in Figure 9b. Both results suggest that Zn speciation in the smelter slag is likely dominated by IR_Xglass, followed by ZnS. The difference in the reference material percentages resulting in the best fit for the XANES and EXAFS spectra, and the non-zero residual of both fits, may be attributable to differences among the Zn spectra of different glasses and/or Zn in solid solutions with spinels and/or FeO (Manceau et al., 2000, Sobanska et al., 2000). It would be difficult to prepare reference materials to resolve these differences, and is arguably unnecessary, as the current results are consistent in their indication of Zn speciation, including S XAS (4.2).

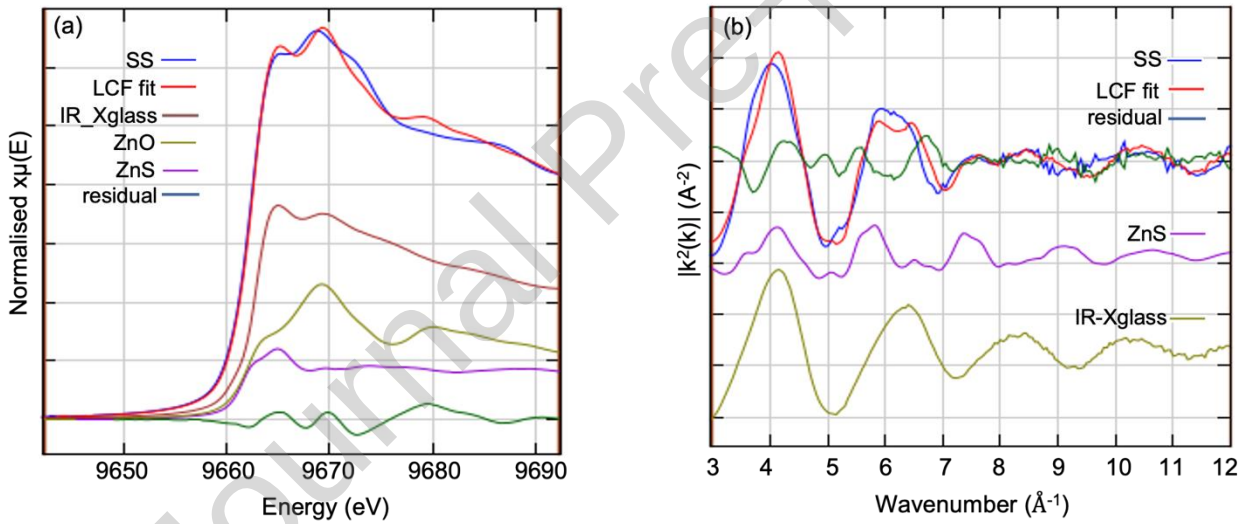


Figure 9. Results of linear combination fit (LCF) for the Zn K-edge XANES (a) and EXAFS (b) spectra of Pb/Zn smelter slag with reference materials selected by fingerprinting. Fit range: -20-30 eV for XANES and 3-12 $Å^{-1}$ for EXAFS.

## 4.4. Pb L3-edge X-ray absorption near edge spectroscopy

### 4.4.1. Fingerprinting and fitting of Pb/Zn smelter slag spectrum with Pb reference material spectra

Figure 10a shows the Pb L3-edge XANES spectrum of the smelter slag sample, compared with those of the eight Pb reference materials with various coordination geometries. The smelter slag and most of the Pb reference materials all have a similar flat peak at the top of the absorption edge, making their contributions to Pb speciation in the slag hard to discern, although the Pb spectrum is distinguished by two peaks at 13043.3 eV ('a') and 13056.6 eV ('b'), and PbO and $PbSO_4$ spectra have peaks at 13054.4 eV ('c') and 13044.6 eV ('d'), respectively. To better identify the Pb speciation, the first derivatives of the Pb L3-edge XANES spectra for the sample slag and the eight reference materials were

compared (Figure 10b). The derivative spectrum of the smelter slag has a dominant peak at 13037.1 eV ('e') after the shoulder at ~13030.0 eV ('f'). This peak and shoulder resemble those of glass (i.e., Corning glasses B and C), and lead apatite (i.e., $Pb_5(AsO_4)_3Cl$ and $Pb_5(PO_4)_3Cl$).

To identify and quantify the Pb phases, LCF was undertaken to fit the first derivative of the Pb L3-edge XANES spectrum of the slag sample using the Pb reference materials identified by fingerprinting (Figure 10c). The best fit result with an R-factor of 0.003 demonstrates a good fit of the spectrum by 60±4% Corning glass B, 29±3% $Pb_5(PO_4)_3Cl$ and 10±2% $PbSO_4$. Although the available lead apatite reference material used in this work contained chloride (2-3 %), the concentration of chlorine in the slag was below the limit for detection by XRF (<0.00087 %). It therefore seems likely that lead is in fact taken up by the hydroxyapatite observed by P XAS (4.2), as has been simulated with FDMNES (Bunău et al., 2021) to show a similar spectrum.

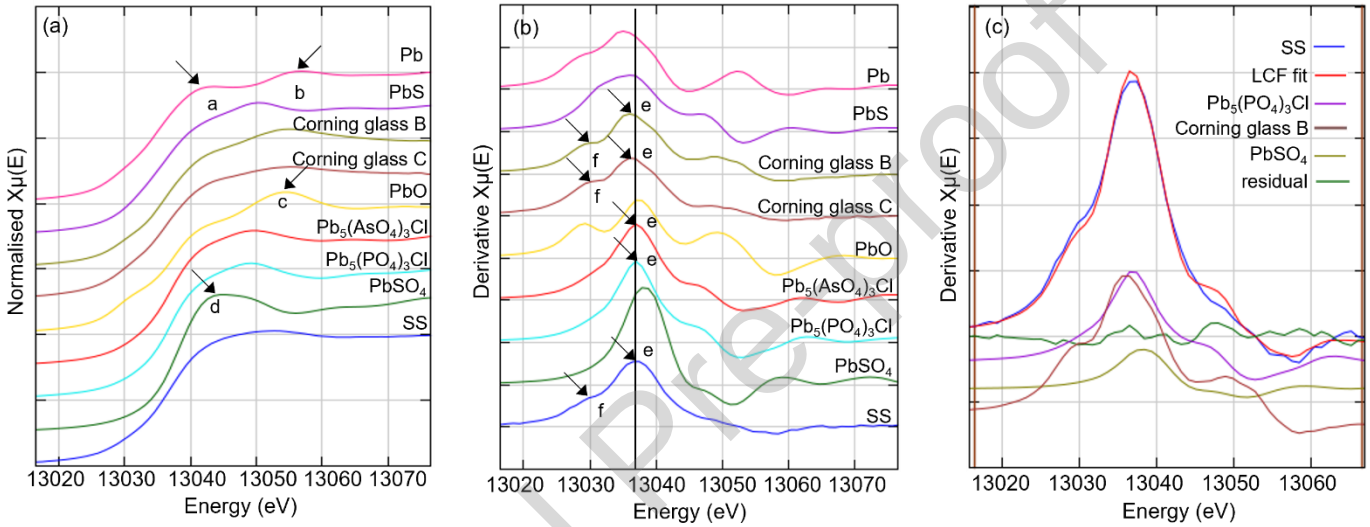


Figure 10. Normalised XANES (a) and first derivatives (b) of Pb L3-edge spectra for the Pb/Zn smelter slag sample and the eight Pb reference materials; Result of its Linear combination fit using those of the Pb reference materials suggested by fingerprinting (c; fit range: -20-30 eV).

## 4.5. Cu K-edge X-ray absorption spectroscopy

### 4.5.1. Edge energy $E_0$

Figure 11 shows Cu oxidation states plotted against Cu K-edge absorption energy $E_0$ for the smelter slag sample and the ten Cu reference materials chosen based on previous studies. The $E_0$ increases from 8979.0 eV to 8987.2 eV and is higher for an oxidation state of +2. The $E_0$ of Cu in Corning glass B is close to that in CuS, in which Cu has a mix of +1 and +2 oxidation states, while that of Cu in the smelter slag sample is between those of $Cu_2O$ and $Cu_2S$ but much smaller than that of CuO. Thus, Cu in Corning glass B likely has a mixed oxidation state of +1 and +2, and the oxidation state of Cu in the smelter slag is likely to be +1.

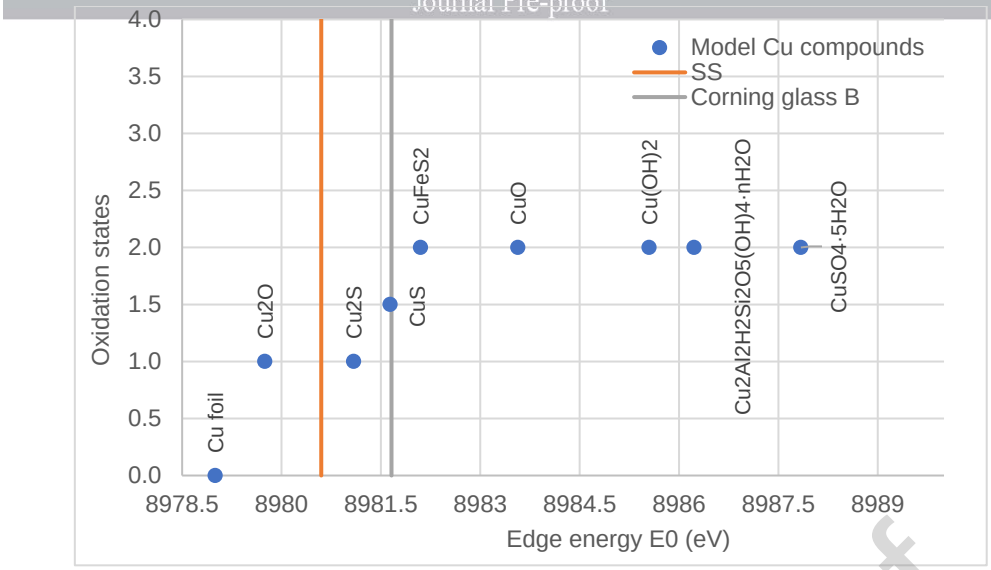


Figure 11. Absorption edge energy $E_0$ of Cu K-edge XAS for the Pb/Zn smelter slag (SS) against oxidation states, compared with all ten Cu reference materials. $Cu_2O$ and $Cu_2S$ edge energies were collected from Gaur et al. (2009) and Newville (2020), respectively.

### 4.5.2. Fingerprinting and fitting of Pb/Zn smelter slag spectra with Cu reference material spectra

Figure 12a shows the normalised Cu K-edge XANES spectrum of the Pb/Zn smelter slag, compared with those of six Cu reference materials with various oxidation states. $Cu(OH)_2$ represents other Cu reference materials with an oxidation state of +2, which have similarly intense peaks at 8994.6-8997.6 eV. Clearly differing from that of $Cu(OH)_2$, the smelter slag spectrum has a flat peak, showing most similarity to that of $Cu_2S$. Although the spectrum of CuS is close to that of the slag, the minor peak at 8986.1 eV ('a') in the CuS spectrum does not appear in the spectrum of the slag.

Figure 12b and c show the Cu K-edge EXAFS and magnitude of the Fourier transform spectra with a k-weight of 2 measured for the smelter slag and five Cu reference materials. In Figure 12b, the EXAFS spectrum of the smelter slag sample has a single sinusoidal oscillation, which, however, does not seem to resemble those of any of the reference materials, even that of $Cu_2S$ (see lines B-E in Figure 12b). Some patterns in the slag spectrum seem to correspond to those of metallic Cu (see lines B-D in Figure 12b). Cu may be present in more than one phase.

The single oscillation corresponds well with a dominant peak at 1.95 in the first coordination shell of its Fourier transform, followed by a broad and weak peak at 4.0-5.0 Å in the second coordination shell (Figure 12c). The distance of the first peak ('f') in the Fourier Transform spectrum of the slag sample is closest to those of $Cu_2S$ and CuS (see line F in Figure 12c). The shallower rising gradient of this peak in the spectrum of the slag differs from those of $Cu_2S$ and CuS, but may be attributable to the divalent Cu reference materials, e.g., $Cu(OH)_2$ or glass, which have closer distances. A broad peak ('h') of the slag is likely contributed by metallic Cu (see line H in Figure 12c), corresponding to the observation made for the EXAFS spectra.

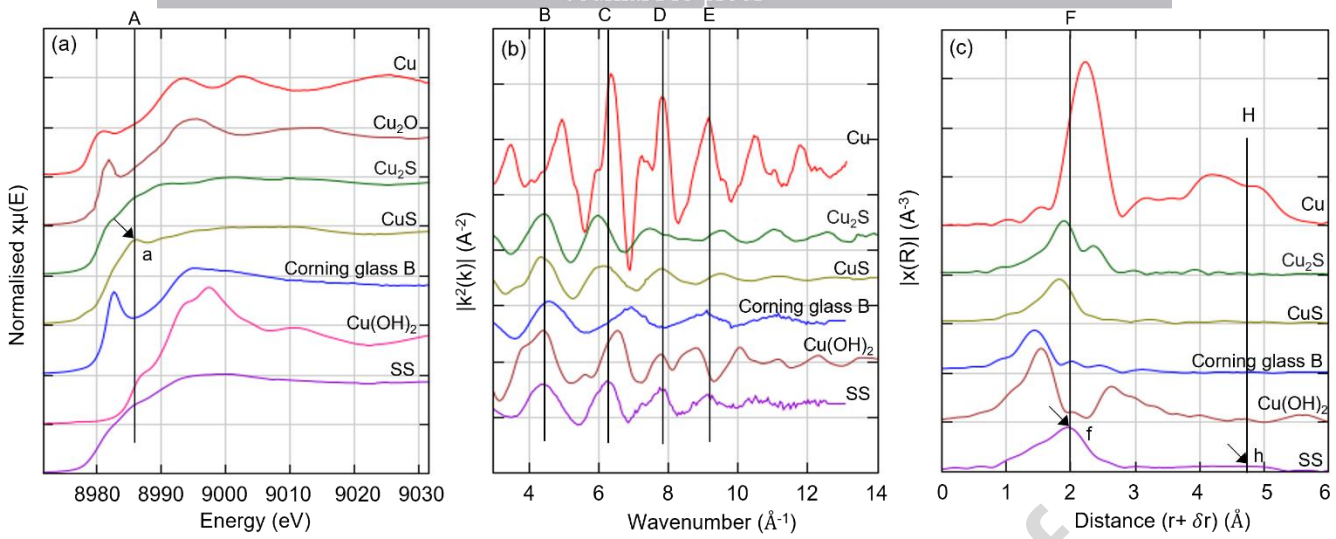


Figure 12. Cu K-edge XANES spectrum of Pb/Zn smelter slag, compared with those of six Cu reference materials (a). Experimental Cu K-edge EXAFS spectra (b) and magnitude of Fourier Transforms (c) for Pb/Zn smelter slag and five Cu reference materials (Fourier Transform spectra are uncorrected for phase shift).

To estimate the quantities of the major Cu phases in the slag sample, LCF of its Cu K-edge XANES, its first derivative, and the EXAFS spectra with the spectra of the Cu reference materials suggested by the fingerprinting was undertaken. In Figure 13a, the best fit result of the Cu K-edge XANES spectrum with an R-factor of 0.0004 demonstrates a good fit of the spectrum by 71±1% $Cu_2S$, 14±1% metallic Cu, and 14±1% $Cu(OH)_2$. The best fit of the first derivative of the Cu K-edge XANES spectrum for the slag resulted in an R-factor of 0.03. This indicates a good fit of the spectrum by 69±2% $Cu_2S$, 14±2% metallic Cu, and 13±1% $Cu(OH)_2$ in Figure 13b. In Figure 13c, the best fit result with an R-factor of 0.08 demonstrates a good fit of the EXAFS spectrum by 65±5% $Cu_2S$, 16±1% metallic Cu, and 19±1% $Cu(OH)_2$.

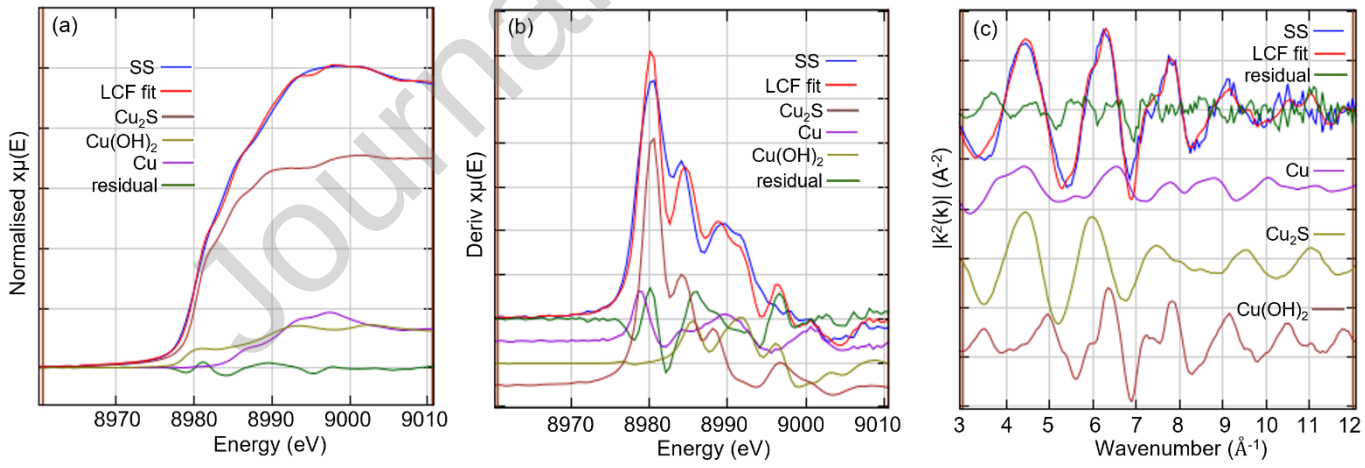


Figure 13. Results of linear combination fitting for Cu K-edge XANES (a) and the first derivative (b) of its XANES spectra, and EXAFS spectra (c) of the Pb/Zn smelter slag with Cu reference materials suggested by fingerprinting. Fit range: -20-30 eV.

## 4.6. As K-edge X-ray absorption spectroscopy result of As

### 4.6.1. Edge energy $E_0$

The edge energy $E_0$ against oxidation states for As in the slag sample and eight As reference materials, which were chosen based on previous studies, is shown in Figure 14, five of which have a valency of +5, two of which have an

oxidation state of +3 ($As_2S_3$ and $As_2O_3$) and one of which has an oxidation state of +0 (As). The $E_0$ increases from 11866.5 eV to 11876.1 eV with an increase in oxidation state from 0 to +5. Compared to $As_2S_3$, $As_2O_3$ has a higher $E_0$ (+4.0 eV). This can be qualitatively explained by the larger attraction between an electron and the nucleus compared to its attraction of oxygen ion at the same oxidation state. The same $E_0$ shift has also been observed in previous studies (Monico et al., 2022). Arsenic in our Pb/Zn smelter slag has a relatively lower $E_0$ of 11869.7 eV, suggesting that its average oxidation state is likely close to +3.

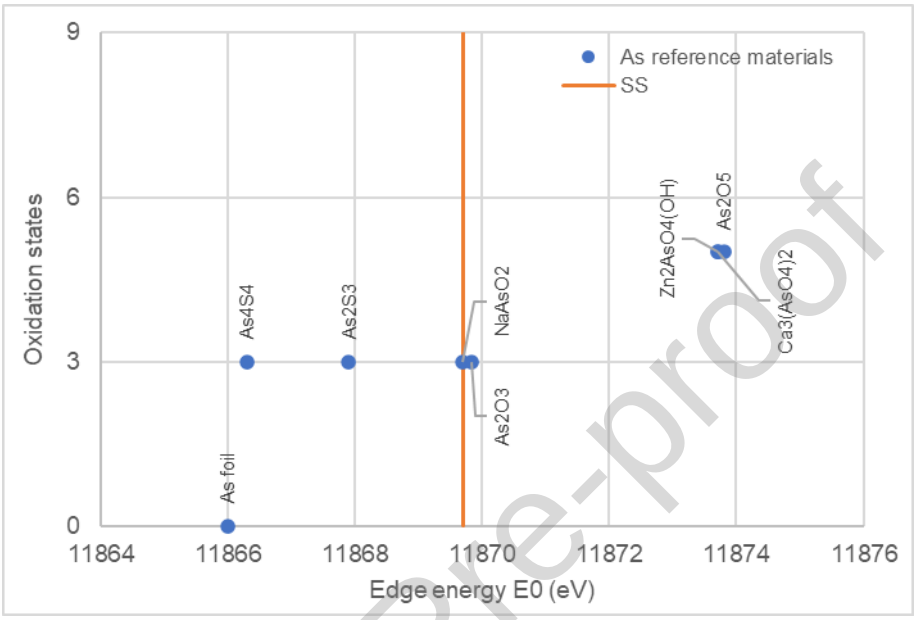


Figure 14. Absorption edge energy $E_0$ of As K-edge XAS for the Pb/Zn smelter slag (SS) against oxidation states, compared with all eight As reference materials.

### 4.6.2. Fingerprinting and fitting of Pb/Zn smelter slag spectrum with As reference material spectra

Figure 15a shows the As K-edge XANES spectrum of the Pb/Zn smelter slag sample, compared with the eight As reference materials. The XANES spectra of all As reference materials have an intense peak, except for that for metallic As, which has a broader and weaker peak. The XANES spectrum of the slag has two peaks at 11872.4 eV ('b') and 11874.9 eV ('c') and a shoulder at ~11868 ('a'). The shoulder 'a' corresponds to AsS (see line A), peak 'b' corresponds to $NaAsO_2$ and $As_2O_3$ (see line B), peak 'c' corresponds to $Ca_3(As(V)O_4)$, $Zn_2As(V)O_4(OH)$ and $As_2O_5$ (see line C).

To estimate the quantities of the major As phases in sample slag, LCF of its As K-edge XANES spectrum with those of the As reference materials suggested by the fingerprinting was undertaken. In Figure 15b, an R value of 0.005 demonstrates a good fit of the spectrum for XANES of sample slag by 51±1% $NaAsO_2$, 28±1% $As_2O_5$ and 21±4% AsS.

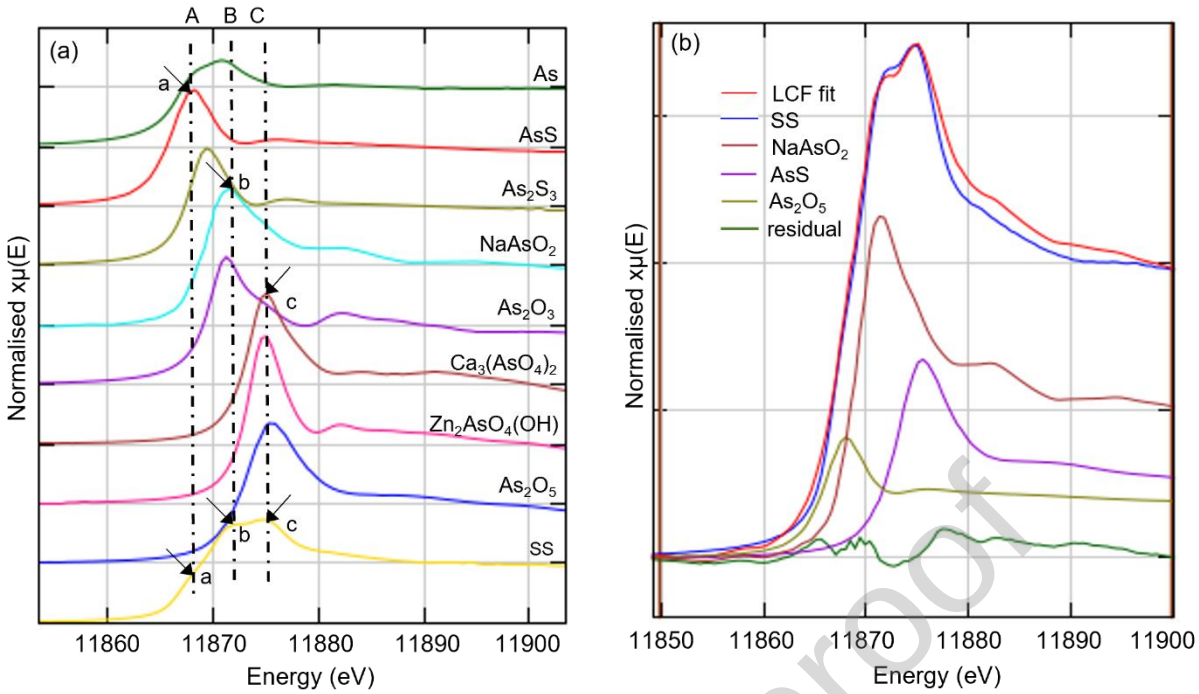


Figure 15. Normalised As K-edge XANES spectra of the Pb/Zn smelter slag and eight As reference materials (a), and result of linear combination fitting using the As reference materials suggested by fingerprinting. Fit range: -20-30 eV (b).

## 5. Discussion

The median Pb/Zn smelter slag contents of Zn, Pb, Cu and As (7%, 0.7%, 0.4% and 0.2 % by mass, respectively) suggest that the 1 Mt/y of Pb/Zn smelter slag that continue to be produced worldwide are a source of 70, 7, 4 and 2 kt/y of Zn, Pb, Cu and As. These elements could potentially be recovered from this waste, or could otherwise gradually leach into the environment, at a rate dependent on their solubility and the slag disposal conditions. Both the recovery and environmental leachability of elements from slag are closely linked to solid phase speciation.

The Pb/Zn smelter slag investigated in our study mostly consists of crystalline wüstite and Ca- and Fe rich silicate glass with a low degree of polymerisation. Wüstite was the only phase detected by XRD, but Fe K-edge XANES showed that the iron is also present as magnetite, and in the glass. The reducing atmosphere in the furnace explains the dominance of the reduced oxidation state of iron ($Fe^{2+}$) in the smelter slag. The SEM/EDS results indicated that the glassy matrix also contains Ca, Fe, and Zn, along with other elements (e.g., S) at lower concentrations. A major fraction of the sulfur in the slag is in glass, its speciation being similar to that of sulfur in GGBFS.

XRF showed 8.4% Zn by mass in the slag but no crystalline phase containing Zn was detected by XRD. Qualitative and quantitative analysis of Zn K-edge XAS of the slag sample suggests that Zn is not restricted to a single phase, but is likely mainly taken up by the glassy slag, followed by ZnS (also corroborated by S K-edge XANES). The minor gaps presenting in the fitted and experimental spectra of Zn in the slag (Figure 9) are possibly attributable to a solid solution with FeO (suggested by XRD) and/or $Fe_3O_4$ (suggested by Fe K-edge XANES) (Manceau et al., 2000, Sobanska et al., 2000). This is supported by the SEM/EDS observation of tiny crystals containing mainly Fe and Zn. The solid solution of Zn in crystalline FeO, however, is excluded based on the fact that edge shift between Fe XANES spectra for FeO and FeO substituted by Zn atoms was absent in the slag spectrum. The solid solution of Zn in $Fe_3O_4$ is also supported by the fact that the second peak in the Fourier Transform spectrum of Zn K-edge EXAFS for nano $ZnFe_2O_4$ shifted to a closer distance to that of the slag ('g' in Figure 8c), observed by Akhtar and Nadeem (2008). Zn, like Fe, can be taken

up in aluminosilicate phases, such as glass or other minerals, during high temperature roasting (Ettler et al., 2020, Li et al., 2017, Hu et al., 2014, Ettler and Johan, 2014, Piatak and Seal II, 2010, Ettler et al., 2009, Puziewicz et al., 2007). ZnS is remaining from the concentrate, and solid solutions of Zn and $Fe_3O_4$ could be formed during roasting.

Analysis of the Pb L3-edge XANES spectrum of the slag in comparison with those of reference materials suggested that Pb was mainly present in glass and apatite, with some lead sulfate. Pb, with a large ionic radius, is more readily taken up by silicate glass than common silicates or oxides (Ettler et al., 2020), as was also observed by SEM/EDS. The presence of apatite was confirmed by qualitative analysis of the P K-edge spectrum of the slag. Either or both Ca and P in apatite are often replaced by other elements, e.g., Pb or As, respectively (Elliott, 1994). The replacement of P by other elements has only a minor influence on the features of Pb XANES spectrum of apatite minerals. For example, the Pb L3-edge XANES spectra of $Pb_5(PO_4)_3Cl$ and $Pb_5(AO_4)_3Cl$ resemble each other in current study and its simulation with FDMNES (Bunău et al., 2021) also shows similar spectra.

Cu K-edge XAS analysis of the slag and the reference materials suggested that Cu was mainly present as $Cu_2S$, followed by metallic Cu and $Cu(OH)_2$. Due to the higher affinity of copper for sulfur than oxygen, $Cu_2S$ is more likely to form than copper oxides (Marakushev and Bezmen, 1971), while some metallic Cu could also form in the reduction stage of the smelting process. Formation of some weathering products, e.g., $Cu(OH)_2$ is plausible, since the slag was obtained from a heap exposed to the open air and rain for several decades (Piatak and Seal II, 2010, Nowinska, 2020). However, the small proportion of $Cu(OH)_2$ is consistent with the shiny morphology of the studied slag, and absence of water in the thermal analysis, which suggest that the weathering reaction happens very slowly.

Arsenic K-edge XANES of the slag and the reference materials suggested the presence of As in multiple phases, mainly $NaAsO_2$, followed by $As_2O_5$ and AsS. AsS remains from the concentrate, $As_2O_5$ is formed during roasting, and $NaAsO_2$ could form by the reaction of $As_2O_3$ during weathering. The XAS results correspond well to the XRF results, which found abundant S (1.6 wt.%), relative to Cu (0.48 wt.%) and As (0.45 wt.%), in the slag. SEM-EDS also found Fe sulfide with impurities of As and Cu. However, it is noteworthy that all the species with similar oxidation states for As have similar spectra, so it is difficult to determine which exact species of As(III) and As(V) may be present. This could explain the small gaps between the fitted and experimental As XANES spectra for the slag in Figure 15b.

Systematic examination of literature findings regarding the mineralogy of Pb/Zn smelter slag, Pb smelter slag and Zn slag (Table 1) showed similar minerals containing the major elements for three types of slags, but there was little information about phases containing minor elements due to the detection limits of the characterisation techniques applied (mainly XRD, followed by SEM-EDS, EPMA and Raman spectroscopy). The XAS findings in the current work not only confirm (e.g., ZnS and $Cu_2S$) and expand (e.g., metallic Cu) the results from the literature about crystalline phases, but also bring insights into amorphous materials (e.g., Zn and Pb in Ca- and Fe rich silicate glass) that comprise much of the slag matrix. The element specificity and spatial resolution of XAS provide more quantitative information about the distribution of elements among their various forms, and also oxidation states, in the whole matrix. It, therefore, solves the overlapping problem of quantifying mineral compositions despite the heterogeneity of the slag and also significantly reduces the intensive labour that is required by EPMA or SEM-EDS.

The identified metal speciation in the Pb/Zn slag can not only be used for an assessment of the potential for environmental pollution, but also be a precursor to examination of changes in speciation as a result of treatment of the slag. For example, solidification/stabilization of the slag in cement or co-processing of this waste in a cement kiln depends not only on the concentrations of both useful and toxic elements, but also respeciation of contaminants to a less mobile form. Recovery of valuable elements, e.g., Zn and Pb, to remove hazards in the waste also depends on their speciation. Policy development for waste management also depends on an understanding of waste composition

and contaminant mobility. For example, end-of-waste assessments (in the EU, and presumably elsewhere) need this information to be able to compare wastes intended for utilisation with conventional materials.

## 6. Conclusions

This study found that both Zn and Pb have an oxidation state of +2, but Cu has a mix of 0, +1 and +2 valences and As has a mixed oxidation state of +3 and +5. Zn was mainly present in glass, followed by ZnS and/or solid solutions with spinel $Fe_3O_4$. Pb was identified mainly in the forms of glass and apatite (e.g., $Pb_5(PO_4)_3OH$), and Cu was found mainly in $Cu_2S$, followed by metallic Cu and a weathering product, $Cu(OH)_2$. The dominant As speciation seems to be $NaAsO_2$, arsenic (V) oxides (e.g., $As_2O_5$), and arsenic sulfide (e.g., AsS). It is significant for the development of waste management regulation and/or metal recovery methods (e.g., hydro/pyrometallurgy) that the solubility of the majority of the Zn, Pb and As could be controlled by a change in pH, while the solubility of most of the Cu and some Zn and As can be increased by oxidation. The application of XAS in our study of slag significantly improved our understanding of speciation of the elements of interest at relatively low concentrations in a heterogeneous matrix, regardless of the crystallinity.

## Acknowledgements

The sample preparation was conducted with funding from the UK Engineering and Physical Sciences Research Council (Grant EP/M00337X/1), and we are grateful to the Diamond Light Source for access to Beamline 18 (under proposals SP11156 and SP16153) for the XAS, and to Andy Dent and Gianantonio Cibin for associated assistance and advice. We also appreciate technical assistance in the UCL Environmental Engineering laboratory from Dr Judith Zhou, and with SEM/EDS from Jim Davy in UCL Earth Sciences.

## References

Adamczyk, Z. & Nowak, J. 2013. The change of mineralogical composition of slag furnances in an isolated from environment storage (Przeobrażenia składu fazowego żużli paleniskowych w składowisku izolowanym od środowiska). *Górnictwo i Geologia,* 8**,** 5-16.

Agrawal, A., Sahu, K. K. & Pandey, B. D. 2004. Solid waste management in non-ferrous industries in India. *Resources, Conservation and Recycling,* 42**,** 99-120. https://doi.org/10.1016/j.resconrec.2003.10.004.

Akhtar, M. J. & Nadeem, M. 2008. Structural studies of $ZnFe_2O_4$ nanoparticles by synchrotron X-ray absorption spectroscopy. *Thai Journal of Physics*. https://www.researchgate.net/publication/232244825_Structural_studies_of_ZnFe2O4_nanoparticles_by_synchrotron_X-ray_absorption_spectroscopy

Alex, T. C., Kalinkin, A. M., Nath, S. K., Gurevich, B. I., Kalinkina, E. V., Tyukavkina, V. V. & Kumar, S. 2013. Utilization of zinc slag through geopolymerization: Influence of milling atmosphere. *International Journal of Mineral Processing,* 123**,** 102-107. https://doi.org10.1016/j.minpro.2013.06.001.

Atzeni, C., Massidda, L. & Sanna, U. 1996. Use of granulated slag from lead and zinc processing in concrete technology. *Cement and Concrete Research,* 26**,** 1381-1388. https://doi.org/10.1016/0008-8846(96)00121-4.

Azuma, S. 2007. Zinc-Lead smelting at Hachinohe smelter. *Journal of MMIJ,* 123**,** 661-665.

Babu, V., Kabeer, K. I. S. A. & Vyas, A. K. 2022. A review on the characterization and use of ISF slag as fine aggregate in cement concrete. *Materials Today: Proceedings*. https://doi.org/10.1016/j.matpr.2022.03.281.

Barna, R., Moszkowicz, P. & Gervais, C. 2004. Leaching assessment of road materials containing primary lead and zinc slags. *Waste management,* 24**,** 945-955. https://doi.org/10.1016/j.wasman.2004.07.014.

Bayer Ozturk, Z., Pekkan, K., Tasci, E. & Yilmaz, S. 2020. The effect of granulated lead–zinc slag on aesthetic and microstructural properties of single-fired wall tile glazes. *Journal of the Australian Ceramic Society,* 56**,** 609-617. https://doi.org/10.1007/s41779-019-00372-0.

Bernasowski, M., Klimczyk, A. & Stachura, R. 2017. Overview of zinc production in imperial smelting process. *Iron and Steelmaking*. https://malzemeciamca.com/wp-content/uploads/2021/06/wp-1623195093567.pdf

Bogush, A., Stegemann, J. A. & Roy, A. 2019. Changes in composition and lead speciation due to water washing of air pollution control residue from municipal waste incineration. *Journal of hazardous materials,* 361**,** 187-199. https://doi.org/10.1016/j.jhazmat.2018.08.051.

Bunău, O., Ramos, A. Y. & Joly, Y. 2021. The FDMNES code. https://doi.org/10.1107/S1574870720003304.

Calvin, S. 2013. *XAFS for Everyone*, CRC press.

Carpenter, P., Counce, D., Kluk, E. & Nabelek, C. 2002. Characterization of Corning EPMA standard glasses 95IRV, 95IRW, and 95IRX. *Journal of Research of the National Institute of Standards and Technology,* 107**,** 703. https://doi.org/10.6028/jres.107.057.

Chen, D. T., Au, W. Y., van Ewijk, S., Roy, A. & Stegemann, J. A. 2021. Elemental and mineralogical composition of metal-bearing neutralisation sludges, and zinc speciation – A review. *Journal of Hazardous Materials,* 416**,** 125676. https://doi.org/10.1016/j.jhazmat.2021.125676.

Commission Decision 2000/532/EC. Commission Decision of 3 May 2000 replacing Decision 94/3/EC establishing a list of wastes pursuant to Article 1(a) of Council Directive 75/442/EEC on waste and Council Decision 94/904/EC establishing a list of hazardous waste pursuant to Article 1(4) of Council Directive 91/689/EEC on hazardous waste. Commission Decision of 3 May 2000 replacing Decision 94/3/EC establishing a list of wastes pursuant to Article 1(a) of Council Directive 75/442/EEC on waste and Council Decision 94/904/EC establishing a list of hazardous waste pursuant to Article 1(4) of Council Directive 91/689/EEC on hazardous waste. https://eur-lex.europa.eu/legal-content/EN/TXT/?uri=CELEX:02000D0532-20150601

Cusano, G., Gonzalo, M., Farrell, F., Remus, R., Roudier, S. & Sancho, L. D. 2017. Best available techniques (BAT) reference document for the non-ferrous metals industries. *Integrated Pollution Prevention Control*. https://EconPapers.repec.org/RePEc:ipt:iptwpa:jrc107041

de Andrade Lima, L. & Bernardez, L. 2011. Characterization of the lead smelter slag in Santo Amaro, Bahia, Brazil. *Journal of Hazardous Materials,* 189**,** 692-699. https://doi.org/11.02.091.

De Angelis, G. & Medici, F. 2012. Reuse of slags containing lead and zinc as aggregate in a Portland cement matrix. *The Journal of Solid Waste Technology and Management,* 38**,** 117-123. https://doi.org/10.5276/JSWTM.2012.17.

Dent, A. J., Cibin, G., Ramos, S., Smith, A. D., Scott, S. M., Varandas, L., Pearson, M. R., Krumpa, N. A., Jones, C. P. & Robbins, P. E. 2009. B18: A core XAS spectroscopy beamline for Diamond. *Journal of Physics: Conference Series,* 190**,** 012039. https://doi.org/10.1088/1742-6596/190/1/012039.

Elliott, J. 1994. *Handbook of structure and chemistry of the apatite and other calcium orthophosphates.* , Elsevier Science: BV.

Ettler, V., Jarošíková, A., Mihaljevič, M., Kříbek, B., Nyambe, I., Kamona, F. & Mapani, B. 2020. Vanadium in slags from smelting of African Pb-Zn vanadate ores: Mineralogy, extractability and potential recovery. *Journal of Geochemical Exploration,* 218**,** 106631. https://doi.org/10.1016/j.gexplo.2020.106631.

Ettler, V. & Johan, Z. 2014. 12 years of leaching of contaminants from Pb smelter slags: Geochemical/mineralogical controls and slag recycling potential. *Applied Geochemistry,* 40**,** 97-103. https://doi.org/10.1016/j.apgeochem.2013.11.001.

Ettler, V., Johan, Z., Kříbek, B., Šebek, O. & Mihaljevič, M. 2009. Mineralogy and environmental stability of slags from the Tsumeb smelter, Namibia. *Applied Geochemistry,* 24**,** 1-15. https://doi.org/10.1016/j.apgeochem.2008.10.003.

Ettler, V. c., Legendre, O., Bodénan, F. o. & Touray, J.-C. 2001. Primary phases and natural weathering of old lead-zinc pyrometallurgical slag from Pribram, Czech Republic. *The Canadian Mineralogist,* 39**,** 873-888. https://doi.org/10.2113/gscanmin.39.3.873.

Franke, R. & Hormes, J. 1995. The P K-near edge absorption spectra of phosphates. *Physica B: Condensed Matter,* 216**,** 85-95. https://doi.org/10.1016/0921-4526(95)00446-7.

Garside, M. 2022. *China's zinc production volume 2010-2021* [Online]. US Geological Survey. Available: https://www.statista.com/statistics/449056/china-zinc-production/ [Accessed].

Gaur, A., Shrivastava, B. & Joshi, S. Copper K-edge XANES of Cu (I) and Cu (II) oxide mixtures. Journal of Physics: Conference Series, 2009. IOP Publishing, 012084.

Gigon, J., Deloule, E., Mercadier, J., Huston, D. L., Richard, A., Annesley, I. R., Wygralak, A. S., Skirrow, R. G., Mernagh, T. P. & Masterman, K. 2020. Tracing metal sources for the giant McArthur River Zn-Pb deposit (Australia) using lead isotopes. *Geology,* 48**,** 478-482. https://doi.org/10.1130/G47001.1.

Giuli, G., Pratesi, G., Cipriani, C. & Paris, E. 2002. Iron local structure in tektites and impact glasses by extended X-ray absorption fine structure and high-resolution X-ray absorption near-edge structure spectroscopy. *Geochimica et Cosmochimica Acta,* 66**,** 4347-4353. https://doi.org/10.1016/S0016-7037(02)01030-X.

Helios-Rybicka, E. W., Rafal 1997. Leaching of Zn, Pd and Cd from metallurgical slag before and after immobilisation. *Geologica Carpathica: Clays***,** 83-89.

Hu, H., Deng, Q., Li, C., Xie, Y., Dong, Z. & Zhang, W. 2014. The recovery of Zn and Pb and the manufacture of lightweight bricks from zinc smelting slag and clay. *Journal of Hazardous Materials,* 271**,** 220-227. https://doi.org/10.1016/j.jhazmat.2014.01.035.

ILZSG. 2022. *Lead and zinc statistics* [Online]. the International Lead and Zinc Study Group (ILZSG). Available: https://www.ilzsg.org/static/statistics.aspx?from=1 Access Date: 2022.

Kas, J., Vila, F., Pemmaraju, C., Tan, T. & Rehr, J. 2021. Advanced calculations of X-ray spectroscopies with FEFF10 and Corvus. *Journal of Synchrotron Radiation,* 28**,** 1801-1810. https://doi.org/10.1107/S1600577521008614.

Kicińska, A. 2020. Physical and chemical characteristics of slag produced during Pb refining and the environmental risk associated with the storage of slag. *Environmental Geochemistry Health***,** 1-19. https://doi.org/10.1007/s10653-020-00738-5.

Kore, S. D. 2020. Performance of Concrete Mixes Using Marble Waste and ISF Slag. https://doi.org/10.23880/oajwx-16000139.

Leng, L., Bogush, A. A., Roy, A. & Stegemann, J. A. 2019. Characterisation of ashes from waste biomass power plants and phosphorus recovery. *Science of the Total Environment,* 690**,** 573-583. https://doi.org/10.1016/j.scitotenv.2019.06.312.

Leuchtenmueller, M., Schatzmann, W. & Steinlechner, S. 2020. A kinetic study to recover valuables from hazardous ISF slag. *Journal of Environmental Chemical Engineering,* 8**,** 103976. https://doi.org/10.1016/j.jece.2020.103976.

Li, Y., Liu, Z., Liu, H. & Peng, B. 2017. Clean strengthening reduction of lead and zinc from smelting waste slag by iron oxide. *Journal of Cleaner Production,* 143**,** 311-318. https://doi.org/10.1016/j.jclepro.2016.12.108.

Luo, L. Q., Zheng, B. T. & Wei, C. X. 2019. A review of phase evolution and characteristics during metallurgical reduction of lead-zinc minerals. *China Mining Magazine,* 28**,** 122-130. http://www.chinaminingmagazine.com/uploads/pdf/1632489373078.pdf

Luo, Y., Wu, X., Sun, H. & Wu, Y. 2020. Root-induced changes in aggregation characteristics and potentially toxic elements (PTEs) speciation in a revegetated artificial zinc smelting waste slag site. *Chemosphere,* 243**,** 125414. https://doi.org/10.1016/j.chemosphere.2019.125414.

Manceau, A., Lanson, B., Schlegel, M. L., Harge, J. C., Musso, M., Eybert-Berard, L., Hazemann, J.-L., Chateigner, D. & Lamble, G. M. 2000. Quantitative Zn speciation in smelter-contaminated soils by EXAFS spectroscopy. *American Journal of Science,* 300**,** 289-343. https://doi.org/10.2475/ajs.300.4.289.

Marakushev, A. & Bezmen, N. 1971. Chemical affinity of metals for oxygen and sulfur. *International Geology Review,* 13**,** 1781-1794. https://doi.org/10.1080/00206817109475642.

McKeown, D. A., Muller, I. S., Buechele, A. C. & Pegg, I. L. 2000. Local environment of Zn in zirconium borosilicate glasses determined by X-ray absorption spectroscopy. *Journal of non-crystalline solids,* 261**,** 155-162.

Meek, R. 1979. *Control of Particulate Emissions in the Primary Nonferrous Metals Industries*.

Monico, L., Prati, S., Sciutto, G., Catelli, E., Romani, A., Balbas, D. Q., Li, Z., De Meyer, S., Nuyts, G. & Janssens, K. 2022. Development of a multi-method analytical approach based on the combination of synchrotron radiation X-ray micro-analytical techniques and vibrational micro-spectroscopy methods to unveil the causes and mechanism of darkening of “fake-gilded” decorations in a Cimabue painting. *Journal of Analytical Atomic Spectrometry,* 37**,** 114-129. https://doi.org/10.1039/D1JA00271F.

Morgan, S. 1968. The place of the Imperial Smelting Process in non-ferrous metallurgy. http://eprints.nmlindia.org/4462

Morrison, A. L., Swierczek, Z. & Gulson, B. L. 2016. Visualisation and quantification of heavy metal accessibility in smelter slags: The influence of morphology on availability. *Environmental Pollution,* 210**,** 271-281. https://doi.org/10.1016/j.envpol.2015.11.030.

Morrison, C., Hooper, R. & Lardner, K. 2003. The use of ferro-silicate slag from ISF zinc production as a sand replacement in concrete. *Cement and Concrete Research,* 33**,** 2085-2089. https://doi.org/10.1016/S0008-8846(03)00234-5.

Nath, S. K. 2020. Fly ash and zinc slag blended geopolymer: Immobilization of hazardous materials and development of paving blocks. *Journal of Hazardous Materials,* 387**,** 121673. https://doi.org/10.1016/j.jhazmat.2019.121673.

Newville, M. 2020. *IXAS X-ray absorption data library* [Online]. Available: https://www.xaslib.xrayabsorption.org/spectrum/86/ Access Date: 08/122022.

Nowinska, K. 2020. Mineralogical and chemical characteristics of slags from the pyrometallurgical extraction of zinc and lead. *Minerals,* 10**,** 371. https://doi.org/10.3390/min10040371.

Nowińska, K. & Zdzisław, A. 2017. Slags of the Imperial Smelting Process for Zn and Pb Production. *Reference Module in Materials Science and Materials Engineering.* Elsevier.

Onisei, S., Pontikes, Y., Van Gerven, T., Angelopoulos, G., Velea, T., Predica, V. & Moldovan, P. 2012. Synthesis of inorganic polymers using fly ash and primary lead slag. *Journal of hazardous materials,* 205**,** 101-110. https://doi.org/10.1016/j.jhazmat.2011.12.039.

Patil, S., Vyas, A., Gupta, A., Vyas, R., Bansal, R. & Patil, R. S. 2018. Desorption Behaviour of Pb and Zn from Stabilized Isf Slag in Bituminous Mixes. *The journal of solid waste technology and management,* 44**,** 92-100. https://doi.org/10.5276/JSWTM.2018.92.

Piatak, N. M. & Ettler, V. 2021. *Metallurgical Slags*, Royal Society of Chemistry.

Piatak, N. M. & Seal II, R. R. 2010. Mineralogy and the release of trace elements from slag from the Hegeler Zinc smelter, Illinois (USA). *Applied Geochemistry,* 25**,** 302-320. https://doi.org/10.1016/j.apgeochem.2009.12.001.

Prasad, P. S. & Ramana, G. V. 2016. Imperial smelting furnace (zinc) slag as a structural fill in reinforced soil structures. *Geotextiles and Geomembranes,* 44**,** 406-428. https://doi.org/10.1016/j.geotexmem.2016.01.009.

Puziewicz, J., Zainoun, K. & Bril, H. 2007. Primary phases in pyrometallurgical slags from a zinc-smelting waste dump, Swietochłowice, Upper Silesia, Poland. *The Canadian Mineralogist,* 45**,** 1189-1200. https://doi.org/10.2113/gscanmin.45.5.1189.

Ravel, B. & Newville, M. 2005. ATHENA, ARTEMIS, HEPHAESTUS: data analysis for X-ray absorption spectroscopy using IFEFFIT. *Journal of synchrotron radiation,* 12**,** 537-541. https://doi.org/10.1107/S0909049505012719.

Reddy, V. A., Solanki, C. H., Kumar, S., Reddy, K. R. & Du, Y. J. 2020. Pb-Zn smelter residue (LZSR) stabilized using low-carbon, low-cost limestone-calcined clay cement: leachability, chemical speciation, strength, and microstructure. *Journal of Hazardous Toxic and Radioactive Waste,* 24. https://doi.org/10.1061/(asce)hz.2153-5515.0000552.

Rissler, J., Klementiev, K., Dahl, J., Steenari, B.-M. & Edo, M. 2020. Identification and quantification of chemical forms of Cu and Zn in MSWI ashes Using XANES. *Energy & Fuels,* 34**,** 14505-14514. https://doi.org/10.1021/acs.energyfuels.0c02226.

Roy, A. 2009. Sulfur speciation in granulated blast furnace slag: An X-ray absorption spectroscopic investigation. *Cement and Concrete Research,* 39**,** 659-663. https://doi.org/10.1016/j.cemconres.2009.05.007.

Roy, A. & Stegemann, J. A. 2017. Nickel speciation in cement-stabilized/solidified metal treatment filtercakes. *Journal of hazardous materials,* 321**,** 353-361. https://doi.org/10.1016/j.jhazmat.2016.09.027.

Sajn, R., Stafilov, T., Boev, B., Serafimovski, T., Tasev, G., Ilijovski, Z. & Boev, I. 2020. Geochemical properties of lead-zinc slag landfill from Mhk Zletovo in Veles, North Macedonia. *Geologica Macedonica,* 34**,** 89-104. https://doi.org/10.46763/GEOL20020089sh.

Sobanska, S., Deneele, D., Barbillat, J. & Ledésert, B. 2016. Natural weathering of slags from primary Pb–Zn smelting as evidenced by Raman microspectroscopy. *Applied Geochemistry,* 64**,** 107-117. https://doi.org/10.1016/j.apgeochem.2015.09.011.

Sobanska, S., Ledésert, B., Deneele, D. & Laboudigue, A. 2000. Alteration in soils of slag particles resulting from lead smelting. *Comptes Rendus de l'Académie des Sciences - Series IIA - Earth and Planetary Science,* 331**,** 271-278. https://doi.org/10.1016/S1251-8050(00)01418-X.

Song, S., Sun, W., Wang, L., Liu, R., Han, H., Hu, Y. & Yang, Y. 2019. Recovery of cobalt and zinc from the leaching solution of zinc smelting slag. *Journal of Environmental Chemical Engineering,* 7**,** 102777. https://doi.org/10.1016/j.jece.2018.11.022.

Sverdrup, H. U., Olafsdottir, A. H. & Ragnarsdottir, K. V. 2019. On the long-term sustainability of copper, zinc and lead supply, using a system dynamics model. *Resources, Conservation & Recycling: X,* 4**,** 100007. https://doi.org/10.1016/j.rcrx.2019.100007.

Taylor, J. C. & Traulsen, H. 1988. World Survey of Nonferrous Smelters. *Phoenix***,** 1988.

Tripathi, B. & Chaudhary, S. 2016. Performance based evaluation of ISF slag as a substitute of natural sand in concrete. *Journal of Cleaner Production,* 112**,** 672-683. https://doi.org/10.1016/j.jclepro.2015.07.120.

Tripathi, B., Misra, A. & Chaudhary, S. 2013. Strength and abrasion characteristics of ISF slag concrete. *Journal of Materials in civil Engineering,* 25**,** 1611-1618. https://doi.org/10.1061/(ASCE)MT.1943-5533.000070.

Tyszka, R., Kierczak, J., Pietranik, A., Ettler, V. & Mihaljevič, M. 2014. Extensive weathering of zinc smelting slag in a heap in Upper Silesia (Poland): Potential environmental risks posed by mechanical disturbance of slag deposits. *Applied Geochemistry,* 40**,** 70-81. https://doi.org/10.1016/j.apgeochem.2013.10.010.

Vanaecker, M., Courtin-Nomade, A., Bril, H., Laureyns, J. & Gouy, S. Evidence of transitional phases during the cooling an, d weathering of Zn in pyrometallurgical slags. *Submitted to European Journal of Mineralogy*.

Vicenzi, E. P., Eggins, S., Logan, A. & Wysoczanski, R. 2002. Microbeam characterization of corning archeological reference glasses: new additions to the smithsonian microbeam standard collection. *Journal of Research of the National Institute of Standards and technology,* 107**,** 719. https://doi.org/10.6028/jres.107.058.

Wang, J., Huang, Q. F., Li, T., Xin, B. P., Chen, S., Guo, X. M., Liu, C. H. & Li, Y. P. 2015. Bioleaching mechanism of Zn, Pb, In, Ag, Cd and As from Pb/Zn smelting slag by autotrophic bacteria. *Journal of Environmental Management,* 159**,** 11-17. https://doi.org/10.1016/j.jenvman.2015.05.013.

Weeks, C., Hand, R. J. & Sharp, J. H. 2008. Retardation of cement hydration caused by heavy metals present in ISF slag used as aggregate. *Cement and Concrete Composites,* 30**,** 970-978. https://doi.org/10.1016/j.cemconcomp.2008.07.005.

Xia, M., Muhammad, F., Zeng, L., Li, S., Huang, X., Jiao, B., Shiau, Y. & Li, D. 2019. Solidification/stabilisation of lead-zinc smelting slag in composite based geopolymer. *Journal of Cleaner Production,* 209**,** 1206-1215. https://doi.org/10.1016/j.jclepro.2018.10.265.

Yang, Y., Li, S., Bi, X., Wu, P., Liu, T., Li, F. & Liu, C. 2010. Lead, Zn, and Cd in slags, stream sediments, and soils in an abandoned Zn smelting region, southwest of China, and Pb and S isotopes as source tracers. *Journal of Soils and Sediments,* 10**,** 1527-1539. https://doi.org/10.1007/s11368-010-0253-z.

Yin, N.-H., Sivry, Y., Guyot, F., Lens, P. N. L. & van Hullebusch, E. D. 2016. Evaluation on chemical stability of lead blast furnace (LBF) and imperial smelting furnace (ISF) slags. *Journal of Environmental Management,* 180**,** 310-323. https://doi.org/10.1016/j.jenvman.2016.05.052.

Zhao, B. 2013. Lead and zinc sintering. *Sintering applications. InTech, Rijeka***,** 165-199. https://books.google.co.uk/books?hl=zh-CN&lr=&id=bOOgDwAAQBAJ&oi=fnd&pg=PA165&dq=Zhao,+B.,+2013,+%27Lead+and+Zinc+Sintering%27&ots=74GwG2zfj3&sig=UvyjWGjOUOOOXR7abrYI6D9NsM4&redir_esc=y#v=onepage&q=Zhao%2C%20B.%2C%202013%2C%20'Lead%20and%20Zinc%20Sintering'&f=false

Zheng, Y.-X., Liu, W., Qin, W.-Q., Han, J.-W., Yang, K., Luo, H.-L. & Wang, D.-W. J. C. M. Q. 2015. Improvement for sulphidation roasting and its application to treat lead smelter slag and zinc recovery. 54**,** 92-100.

Graphical abstract

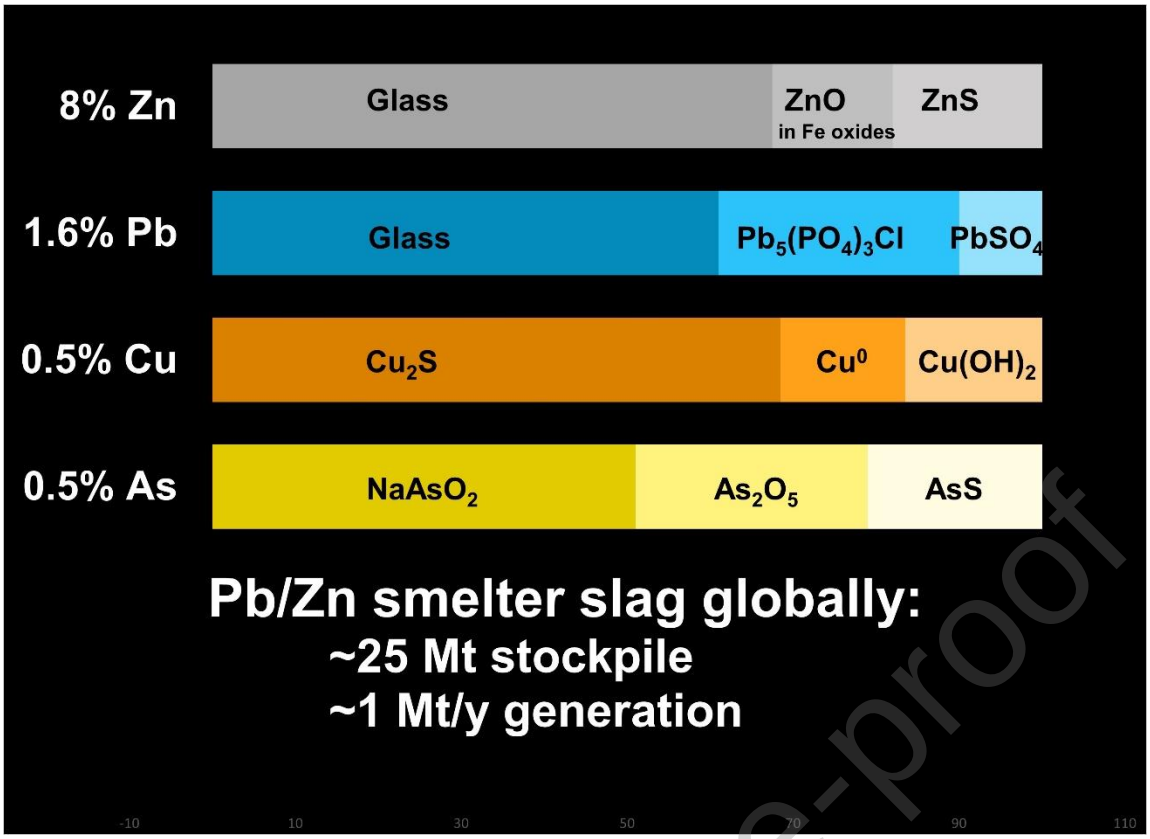


**CRediT author statement**

**Dan Ting Chen:** Writing-original draft, Methodology, Data curation, Formal analysis, Investigation, Visualisation. **Amitava Roy**: Conceptualisation, Resources, Methodology, Formal Analysis, Supervision, Writing-review & editing. **Yu Qian Li**: Formal analysis**. Anna Bogush:** Methodology, Investigation**. Wing Yin Au**: Investigation. **Julia A. Stegemann**: Conceptualisation, Methodology, Writing-review & editing, Supervision, Funding acquisition, Project administration.

**Declaration of interests**

☒ The authors declare that they have no known competing financial interests or personal relationships that could have appeared to influence the work reported in this paper.

☐ The authors declare the following financial interests/personal relationships which may be considered as potential competing interests:

## Environmental Implications

Current production of Pb/Zn smelter slags is about 1Mt/y, and past disposal of more than 25 Mt of these slags has already deposited nearly 2 Mt of zinc, 0.2Mt of lead, 0.1 Mt of copper and 0.05 Mt of arsenic in the environment. These elements could potentially be recovered, or will gradually leach out, depending on their speciation and the disposal conditions. This work has used X-ray absorption spectroscopy to determined the speciation of these elements, which will help to understand the risks these slags pose and develop better disposal, utilisation or element recovery techniques.

## Highlights

- ~1 Mt/y of Pb/Zn smelter slags are a source of 70, 7, 4 and 2 kt/y of Zn, Pb, Cu and As, respectively
- Zinc and lead are both mainly in glass, but also as ZnO or ZnS, or Pb apatite and $PbSO_4$
- Copper is mainly $Cu_2S$, with Cu metal and $Cu(OH)_2$
- Arsenic is mainly in $NaAsO_2$, and also $As_2O_5$ and AsS
- Elucidation of elemental speciation at low concentration in complex matrices by XAS is shown